DEVELOPMENT OF POROUS BIOACTIVE SiO_2-Na_2O-CaO-P_2O_5 GLASS CERAMIC SCAFFOLD

A Thesis Submitted
In Partial Fulfilment of the Requirement
for the degree of
BACHELOR OF TECHNOLOGY

By
Hara Prasad Murty
ROLL 108CR008

TO THE
DEPARTMENT OF CERAMIC ENGINEERING
NATIONAL INSTITUTE OF TECHNOLOGY ROURKELA
MAY 2012

DEVELOPMENT OF POROUS BIOACTIVE SiO_2-Na_2O-CaO-P_2O_5 GLASS CERAMIC SCAFFOLD

A Thesis Submitted
In Partial Fulfilment of the Requirement
for the degree of
BACHELOR OF TECHNOLOGY

By
Hara Prasad Murty
ROLL 108CR008

Supervisor: Dr. Sumit Kumar Pal

TO THE
DEPARTMENT OF CERAMIC ENGINEERING
NATIONAL INSTITUTE OF TECHNOLOGY ROURKELA
MAY 2012

NATIONAL INSTITUTE OF TECHNOLOGY

ROURKELA

CERTIFICATE

This is to certify that the thesis entitled, ***"Development of Porous Bioactive SiO_2-Na_2O-CaO-P_2O_5 Glass Ceramic Scaffold"*** submitted by ***Mr. Hara Prasad Murty (108CR008)*** in partial fulfilments for the requirements for the award of ***Bachelor of Technology*** degree in ***Ceramic Engineering*** at National Institute of Technology, Rourkela is an authentic work carried out by him under my supervision and guidance.

To the best of my knowledge, the matter embodied in this thesis has not been submitted to any other University/Institute for the award of any Degree or Diploma.

Date:

Dr. Sumit Kumar Pal
Assistant Professor
Department of Ceramic Engineering
National Institute of Technology
Rourkela – 769008

ACKNOWLEDGEMENT

With deep respect, I avail this opportunity to express my gratitude to Dr. Sumit Kumar Pal, Assistant Professor, National Institute of Technology, Rourkela for his inspiration and guidance and valuable suggestion throughout this research work. It would have been impossible on my part to come out with this project report without him. I would like to express my gratitude to Dr. Japes Bera, HOD, Ceramic Engineering for permitting to carry out my project. I would like to take this opportunity to thank all the faculty members of Ceramic engineering Department namely Dr. S. Pratihar, Dr. B.B. Nayak, Dr. D. Sarkar, Mr A. Choudhury, Dr. S. Behera, Dr. R. Mazumder, Dr. R. Sarkar, Dr. S. Dasgupta, and Dr. S. Bhattacharyya(Mrs). I would also take this opportunity to express my gratitude to the non-teaching staff Mr P.K. Mohanty, Mr G. Behera, and Mr S. Sahoo for their help and kind support. I would also like to thank Mr Sanjay Swain, Mr Ganesh Sahoo and Mrs Geetanjali Parida(PhD Scholars) for the help and support in carrying out experiments and providing every sort of help possible. And last but not least I am thankful to my friend Mr Udipto Thakur for his constant support and encouragement.

Hara Prasad Murty

108CR008

List of Tables

List of Figures

Contents

Abstract

Bioactive glasses of chemical composition **48.4SiO_2 -23.8Na_2O- 23.8CaO- 4.0P_2O_5** wt% was prepared through Sol-Gel route. It was then crystallized through thermal treatment. Porous samples of the mentioned composition using Naphthalene (0, 30, and 50 weight percentage) as pore former were made and tested for Bulk Density, Apparent porosity, Linear Shrinkage, Cold Crushing Strength, and Bi-axial flexural strength. Maximum porosity of 50% was obtained by this process. The maximum value of CCS obtained was 7.8MPa without any pore former and a minimum of 2.3 MPa for 50% Naphthalene. The Bi-axial flexural strength varied between the extremes of 16.3 MPa and 5.6 MPa. Their pore size distribution was also studied to ensure the presence of pores with size greater than 100 µm, which happens to be the critical lower limit for Angiogenesis. Samples were also prepared with a radial porosity gradient similar to the structure of the cancellous part of the Bone structure. The samples contained a central core of higher porosity and a outer concentric ring of lower porosity. These samples were also tested for the above mentioned mechanical properties. The Bioactivity of the samples was also studied by immersing them in a SBF solution for a period of 1, 3, and 7 days. These samples were then studied using XRD, SEM, EDX, and FTIR and showed significant formation of HCA ensuring their Bioactivity.

CHAPTER 1:
INTRODUCTION

Introduction

Recent developments in tissue engineering in the field of orthopaedic implants look forward to develop the regeneration capabilities of the host tissues using advanced designing methods for preparation of implants to match the structure of the host tissues in order to accelerate the rejuvenation of the damaged tissues. This requires the preparation of implants which are similar to that of the host tissue structure both in terms of structure as well as mechanical and Biological properties. In reference to the above requirements, bioactive glasses have shown promising prospects. Due to their class A bioactivity confirming both osteoconduction and osteoproduction, have become the material of major interest. Since the revolutionising paper by Hench on Bioglass in 70s, the composition has been optimised several times for better results than the last one. The present composition of bioactive glass **1.5N1.5C3S + 4P** is a result of one of such successful endeavour. But in the present Scenario of 3rd generation Implants, the composition itself is not enough for its success. The present study is based on preparing a method for economical production for an implant structure similar to that of **cancellous** part of the bone structure. Cancellous bones have a structure with a radial porosity gradient, with a highly porous central core structure and denser outer concentric ring. The outer structure gives strength to the bone while the inner core provides volume and surface area for hematopoiesis by the bone marrow present in them. Thus the additional restraint on the production of implants for this purpose requires the presence of pores with diameter larger than 100µm for angiogenesis to occur. Angiogenesis is the process of growth of blood vessels and nerve tissues into the structure of these implants. Also the cancellous bones are less dense, softer, weaker, and less stiff than dense cortical bones thus requiring the mechanical properties of the implants to be restrained within the limits of the properties of these bones. Thus the implants for this application require careful engineering of mechanical properties.

Scope of the Project

A glass composition named **1.5N1.5C3S + 4P** [*Oscar Peitl,Edgar D. Zanotto, Francisco C. Serbena b, Larry L. Hench. Acta Biomaterialia 8 (2012) 321–332*] is prepared having the following composition: **48.4SiO_2 -23.8Na_2O- 23.8CaO- 4.0P_2O_5** (wt%) through Sol-Gel route. Then the glass was converted to glass ceramics by heat treating the material at 700^oC for 2hrs.

3.1 Objective of the proposed project

1. Preparation of porous bodies of varying porosities (0%, 30%, 50%) by powder pressing method.
2. Preparation of porous bodies with a porosity gradient with decreasing porosity radially from centre to circumference.
3. Mechanical characterization of the above samples which includes Bulk Density, Apparent Porosity, Cold Crushing Strength, and Biaxial Flexural Strength.
4. Studying the effect of amount of pore-former on pore size.
5. Biological Characterization to check their Bioactivity by immersing the samples in Simulated Body Fluid(SBF) for varying periods and studying the formation of Hydroxy Carbonated Apatite(HCA) layer .

CHAPTER 2:

LITERATURE REVIEW

2.1 Why Bioglass?

The major problem with the 1st generation bio implants was that they were made of either metals or synthetic polymers which was a foreign material for the host tissue and was thus rejected by it, by the formation of scar tissues. Then with the discovery of Bioglass composition in the early 70s this problem was taken care of as the then developed 45S5 composition showed the formation of hydroxyapatite layer in test solutions that did not contain calcium or phosphate ions[1]. As Bioglass shows higher mechanical strength and bioactivity than Hydroxy Apatite (HA), it has become the new favourite in the market triggering larger resources into its development. Bioactive glasses show excellent ability to nurture the growth of new bone cells on their surface.[2,3] When the bioactive glasses are tested in vivo, they undergo specific reactions forming amorphous calcium phosphate(ACP), which causes strong bonding with the host tissue[4]. The release of Ca^{2+} ions by the bioactive glasses has also been reported to activate oestrogenic genes[5].

2.2 Sol-gel processing:

Sol method is preferable over other methods for preparation of Bioactive glasses as it gives better control over homogeneity and purity[6] as both these conditions are very essential in the production of bioactive glasses. Apart from it, this method decreases the processing temperature against orthodox methods like melt quenching. It has also been noticed that 45S5 glass made from sol-gel route showed higher bio activity than the one obtained from melt quenching method. The reactions taking place during the gelation process can be decribed as a condensation reaction transforming TEOS on hydrolysis on reacting with water to form $HSi(OH)_3$, which then condenses to form Si-O-Si bond leading to the growth of a 3 dimensional network structure.

2.3 The mechanism of bioactivity:

The mechanisms of bioactivity and bone bonding have been widely studied [7]. A series of reactions leading to the formation of ACP has been stated to be the primal reason. The mechanism of HCA formation has been described by Hench [7] as a series of surface reactions. These can be summarised as-

Step 1: Rapid ion exchange reactions between the glass network modifiers (Na^+ and Ca^{2+}) with H_3O^+ ions from the solution leading to hydrolysis of the Si groups and the creation of Silanol (Si–OH) groups on the glass surface.

Step 2: The increase in pH causes dissolution of silica, to silicic acid, $Si(OH)_4$, into the solution, and the continued formation of Si–OH groups on the glass surface.

Step 3: Condensation and polymerization of an amorphous SiO_2-rich layer (1-2 micron) on the surface of the glass depleted in Na^+ and Ca^{2+}.

Step 4: Migration of Ca^{2+} and $(PO_4)^{3-}$ ions from the glass through the SiO_2-rich layer and from the solution, leading to the formation of an ACP layer on the surface of the SiO_2-rich layer.

Step 5: The ACP layer incorporates $(OH)^-$ and $(CO_3)^{2-}$ from the solution and crystallizes as an HCA layer.

2.4 Sintering behaviour of Bio active glass:

An important step in studying the bioactive glass is to study its sintering behaviour. The sintering of the sample comprises of the heat treatments done within the temperature range of 550^{o}C to 900^{o}C. Not much composition specific work has been done on this topic except in case of 45S5 glass. But the overall mechanism of the sintering behaviour can be understood by considering a few fundamental points. As it consists of a major glass phase, the dominating sintering mechanism must be the viscous flow. Crystallization in case of

Bioactive glasses starts at as low temperature as 550^{o}C, which causes the formation of crystallites thus impeding the sintering process.

2.5 Structural transformations in a bioactive glass:

The material obtained after drying the gel is an amorphous material. The crystallization temperature of most bioactive glasses is as low as 550^{o}C, so crystalline phases start to appear even before the complete decomposition of the precursors during calcination. The first step in the structural transformation is the first glass transition temperature $Tg_{1,}$ which is followed by glass in glass phase separation leading to the creation of silica and phosphorous rich phase. The crystallization of the bioactive phase $Na_4Ca_4Si_6O_{18}$ takes place. Crystallization of the remaining glassy phase starts after reaching the 2nd glass transition temperature at around 850^{o}C. finally the glass vitrifies and melts at a temperature of 1200-1300^{o}C depending on the composition.

2.6 Functionally graded tissue engineering scaffolds:

Natural Tissues including human bone tissues, display gradients in structure across a spatial volume, which in most of the cases is radial in nature. Each layer has specific functions to perform; so that the whole tissue/organ can behave normally. Such a gradient is termed a functional gradient. A good TE scaffold should imitate such a gradient, which fulfils the biological and mechanical requirements of the host tissue [8]. Computer aided designs are often used for the purpose of easing this task. Rapid prototyping methods are the most advanced in this field.

2.7 Hruby coefficient:

It is a parameter used for evaluating the crystallization ability of glass ceramics [9].

It is given by formula

$Hr= (T_p-T_g)/(T_m-T_p)$

Where

Hr = Hruby coefficient

T_p = peak crystallisation temperature

T_g = glass transition temperature

T_m = onset melting temperature

Hr for standard 45S5 glass is 0.27 but it increases with increase in P_2O_5 content of the composition. The Hruby coefficient of present glass composition was calculated to be 0.5. The higher value is due to the larger amount of Phosphorous.

2.8 Mechanical property requirements for implants replacing cortical and cancellous bones [11]:

	Cortical Bone	Cancellous Bone
CCS (MPa)	100-150	2-12
Flexural Strength (MPa)	135-193	10-20
Tensile Strength (MPa)	50-151	1-5
Elastic Modulus (Gpa)	10-20	0.1-5
Fracture Toughness (MPa-$m^{1/2}$)	2-12	0.1-0.8
Porosity (%)	5-10	50-90

Table 2.1: Mechanical properties of cortical and cancellous bone.

2.9 The influence of the phosphorus content on the bioactivity of sol–gel glass ceramics:

The presence of phosphorous in the glass composition leads to the evolution of a larger number of phases. It helps in stabilizing the wollastanite phase at a higher temperature, which increases the strength. It also induces the formation of apatite and TCP at lower temperatures. The presence of phosphorous increases the bioactivity of the composition, but mean while it also decreases the fracture toughness and other mechanical properties by producing a heterogeneous distribution of defects.

CHAPTER 3:
EXPERIMENTAL DETAILS

3.1 Experimental Work

3.1.1 Material Preparation: The glass of the below mentioned composition(in weight percentage) was prepared through sol gel route as it gives greater control over homogeneity and purity.

Glass Ceramic	SiO_2	Na_2O	CaO	P_2O_5
1.5N1.5C3S + 4P	48.5	23.8	23.8	4

Table 3.1.1: Composition of Glass(wt%)

Raw materials used-

Tetraethoxysilane ($Si(OC_2H_5)_4$), fig. 3.1.1

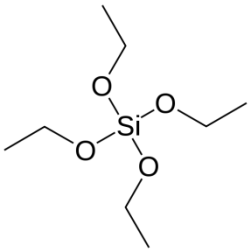

Fig. 3.1.1: TEOS

- Molecular weight 208.33 g mol^{-1}
- Density 0.933 g mL^{-1}
- Smells like spearmint
- Practically insoluble in water. Hydrolyses in water.

Triethyl Phosphate ($OP(OC_2H_5)_3$), fig. 3.1.2

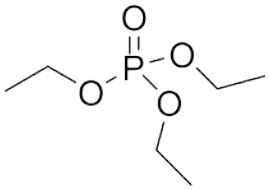

Fig. 3.1.2: TEP

- Molecular weight 182.15 g/mol
- Density 1.072 g/cm^3
- Colourless liquid
- Mild odour

Calcium nitrate tetrahydrate ($Ca(NO_3)_2{\cdot}4H_2O$**),** fig. 3.1.3

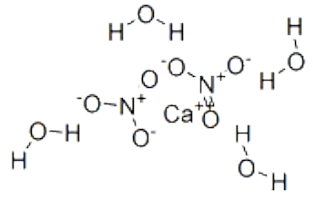

Fig. 3.1.3: Calcium Nitrate

- Molecular weight 236.15 g/mol

- Density 1.896 g/cm^3
- Highly soluble in water.
- Hygroscopic in nature thus required precautions should be taken.

Sodium nitrate ($NaNO_3$) , fig. 3.1.4

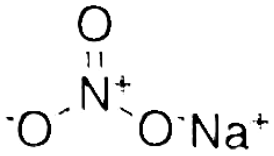

Fig. 3.1.4: Sodium Nitrate

- Molecular weight 84.9947 g/mol
- Density 2.257 g/cm^3; Solid
- Very soluble in ammonia; soluble in alcohol and water.

Ammonia solution (NH_4OH)

- Concentration is 28-30 wt % in water typically
- Molecular weight of NH_4OH is 35.05 g mol^{-1}, Density 0.9 g mL^{-1}
- Form is a pungent liquid that smells like cleaning ammonia, use in a vent hood

Ethanol (C_2H_5OH)

- Molecular weight 46.07 g mol^{-1}
- Density 0.789 g mL^{-1}

Batch calculation- (for 15gm batch)

a) SiO_2(from $Si(OC_2H_5)_4$)

48.4% of 15gm =7.275gm

$Si(OC_2H_5)_4 + 2\ H_2O \rightarrow SiO_2 + 4\ C_2H_5OH$

208.33gm 60.08gm

Weight of TEOS required = 208.33*7.275/60.08=25.2263gm

Density of TEOS is 0.933 g mL^{-1}; so volume required=25.2263/0.933= 27.0379ml

Purity of reagent used is 98%; so adjusted volume= 27.0379/0.98= **27.5879ml**.

b) Na_2O(from $NaNO_3$)

23.8% of 15gm =3.57gm

$2NaNO_3 \rightarrow Na_2O + NO$

2*84.99gm 61.98gm

Weight of $NaNO_3$ required = 2*84.99*3.57/61.98=9.7906gm

Purity of reagent used is 98%; so adjusted weight= 9.7906/0.98= **9.9905gm.**

c) CaO(from $Ca(NO_3)_2 \cdot 4H_2O$)

23.8% of 15gm =3.57gm

$2\ Ca(NO_3)_2.4H_2O \rightarrow 2\ CaO + 4\ NO_2 + O_2 + 8\ H_2O$

236.15gm 56.077gm

Weight of $Ca(NO_3)_2 \cdot 4H_2O$ required = 236.15*3.57/56.077=15.0339gm

Purity of reagent used is 98%; so adjusted weight= 15.0339/0.98= **15.3407gm**

d) P_2O_5(from $OP(OC_2H_5)_3$)

4% of 15gm =0.6gm

$2(C_2H_5)_3PO_4 \rightarrow P_2O_5 +$

2*182.16 283.84/2

Weight of TEP required = 4*182.16*0.6/283.84=1.5402gm

Density of TEP is 1.073gm/mL; so required volume =1.5402/1.073=1.4354mL

Purity of reagent used is 98%; so adjusted volume = 1.4354/0.98= **1.4647mL**

e) Preparation of 2M HNO_3(from 70%v/v reagent)

1 Molar solution =1 molecular wt/lr = 63gm/lr

So, 2M solution = 126gm/lr.

Density of HNO_3 is 1.5129gm/mL; so required volume = 126/1.5129=83.2837mL.

Concentration is 70% v/v; so adjusted volume = 83.2837/0.7= **118.9768ml**

So 129mL of HNO_3 is taken in a volumetric flask and filled up to 1Lr. mark.

Preparation of the gel-

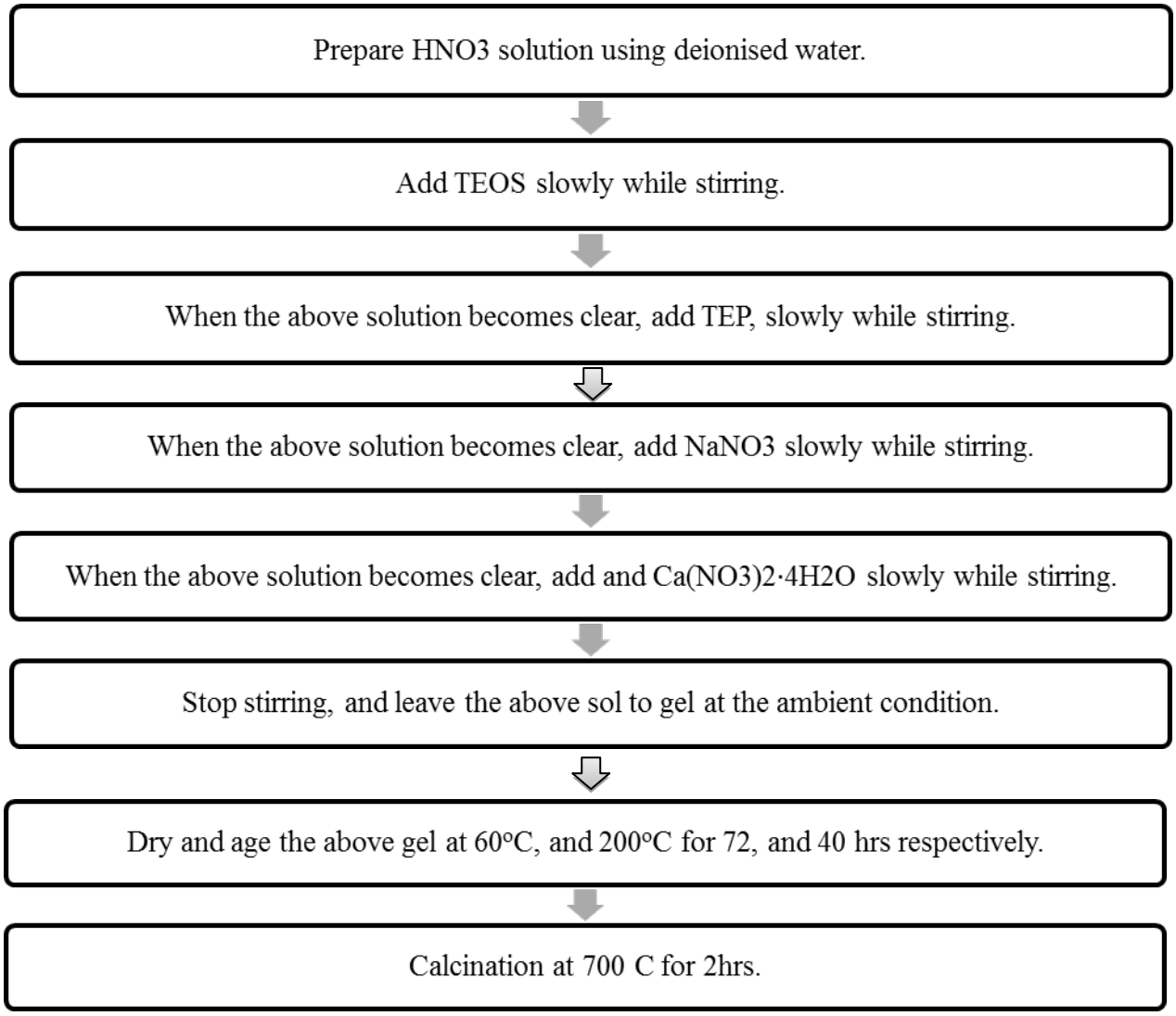

Fig. 3.1.5: Flow chart for the Sol-Gel Route

a) A solution of 2 M HNO_3 is prepared by adding 28 mL HNO_3 (70% v/v) to 250 mL of water.

b) Mix 27.6 mL TEOS and 55 mL Ethanol in a beaker in the ratio 1:2 (v/v) with the help of a magnetic stirrer.

c) Pour 27.6 mL of 2 M HNO_3 solution in the above beaker keeping water: alcohol ratio 1:2 (v/v) and mix the solution with the magnetic stirrer.

d) Add 1.4 mL TEP to the above solution and stir it till the solution becomes clear.

e) Mix 9.9905 grams of $NaNO_3$ with fair amount of alcohol/water in a separate beaker and pour the solution in the above beaker while stirring.

f) When the above solution becomes clear, add 15.0339 $Ca(NO_3)_2 \cdot 4H_2O$ directly, as the salt is hygroscopic in nature and continue stirring till we get a clear solution.

g) This is the “sol”.

h) Gelation takes place over a period of 120 hrs distributed as 72hrs at 60^oC and 40 hrs at 200^oC.

3.1.2 **Milling** of the calcined powder is done for 6 hrs. at 300 rpm using a planetary ball mill. The setup contained two Silicon Nitride containers with Silicon Nitride balls of diameter 20mm (10 nos.) and 5mm (10 nos.). the sample was wet milled using Acetone as the liquid medium. After milling, the slurry was dried in a hot air drier. Then the loosely bound agglomerates were grinded manually using Agate mortar and pestle.

3.1.3 **Preparation of samples**: 3.Samples were made of different compositions by varying the weight percentage of Naphthalene. Compositions of 0%, 30%, and 50%, naphthalene were made and are denoted as 0p, 30p,and 50p respectively These were than latter used to make pellets of uniform porosity and radially graded porosity. 5% Poly Vinyl Alcohol (PVA) was used as a green binder for initial green strength of the pellets. PVA solution was added in an approximate ratio of 1drop per gram of powder. Acetone was used as a mixing aid while adding PVA for more homogeneous distribution of the binder. Pressing was done at 100 MPa and 200 MPa pressures. 2% stearic acid solution was used for lubrication of the die punch arrangement and acetone was used for cleaning the die punch arrangement. Cleaning and lubrication

was done after each pressing.For making pellets of uniform porosity, 0.6gms of sample from each above mentioned category was used to make pellets.

For making pellets with radial distribution of pores, pellets are made in such a way that the inner part has higher porosity as compared to the outer part. In the present work two materials of different porosities are used for making a single pellet. So there are six different combinations possible: 0p/30p, 0p/50p, and 30p/50p. In the above mentioned format, the numerator represents the weight percentage of Naphthalene in the of the outer ring while the denominator represents the weight percentage of Naphthalene in the central part of the pellet. The two materials are divided in such a way that the surface area of the inner ring is a fourth of the total surface area of the pellet as can be seen from a top view. Thus the 0.6 grams of the sample weight is divided into 0.45 grams of the less porous composition and 0.15 gram of higher porous composition.

3.1.4 Pressing technique: in order to make the pellets with porosity gradient, two methods can be followed

a) The total diameter of the green pellet is 12 mm. so another preform of diameter 6 mm in the form of a plastic hollow cylinder was used to fill the material of the inner ring by placing it inside the die-punch setup in such a way that their centres coincide. The material with higher weight percent of naphthalene was filled into the plastic cylinder and the one with lower weight percent of naphthalene was filled in the outer concentric ring bounded by the inner surface of the die and the outer surface of the plastic cylinder as shown in fig 3.1.6(a).

b) In this method a cuboid shaped bar of dimension 35mmX5mmX5mm is made of the material with higher weight percentage of Naphthalene by pressing it at

200KPa and it is cut to the required length so as to match the thickness of the final green pellet. Then this piece of pellet having a square cross section of side 5mm is placed at the centre of the die mould and the material with lower weight percentage of naphthalene is filled in the outer sides as shown in the fig 3.1.6(b).

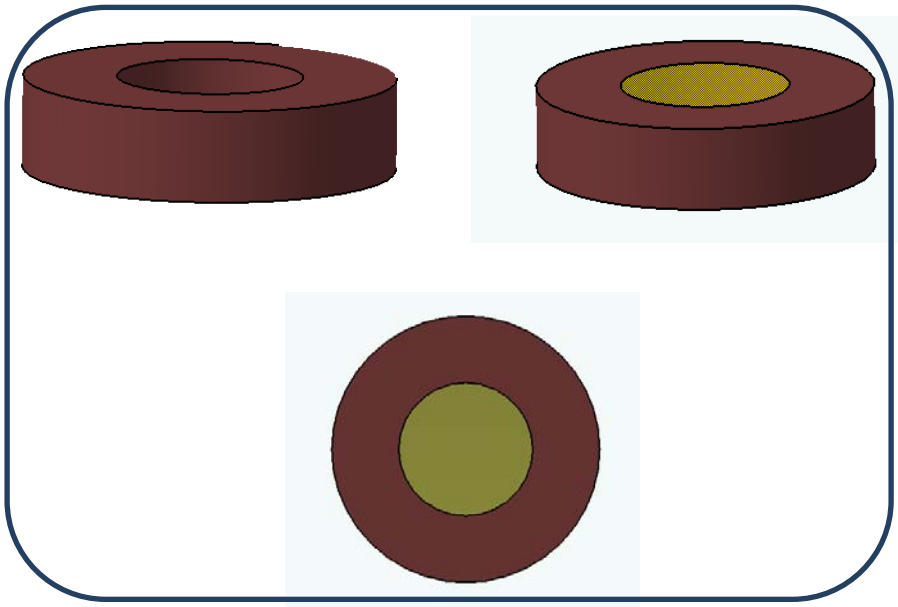

(a)

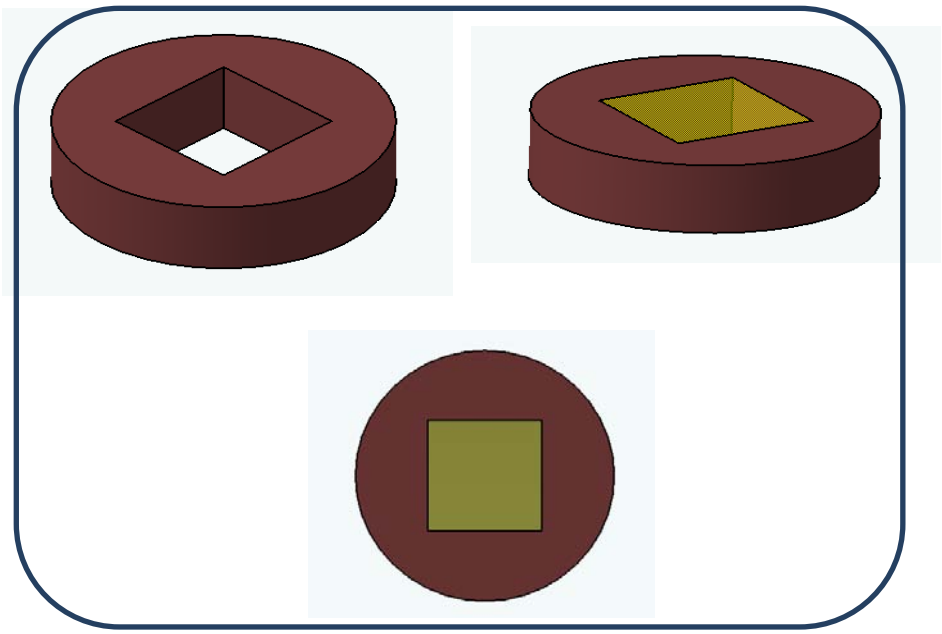

(b)

Fig. 3.1.6: Schematic of the pellets with porosity

3.1.5 Sintering of the samples were done at a temperature of 1050^{o}C. Sintering is done in a closed atmosphere. The sintering profile was as follows:

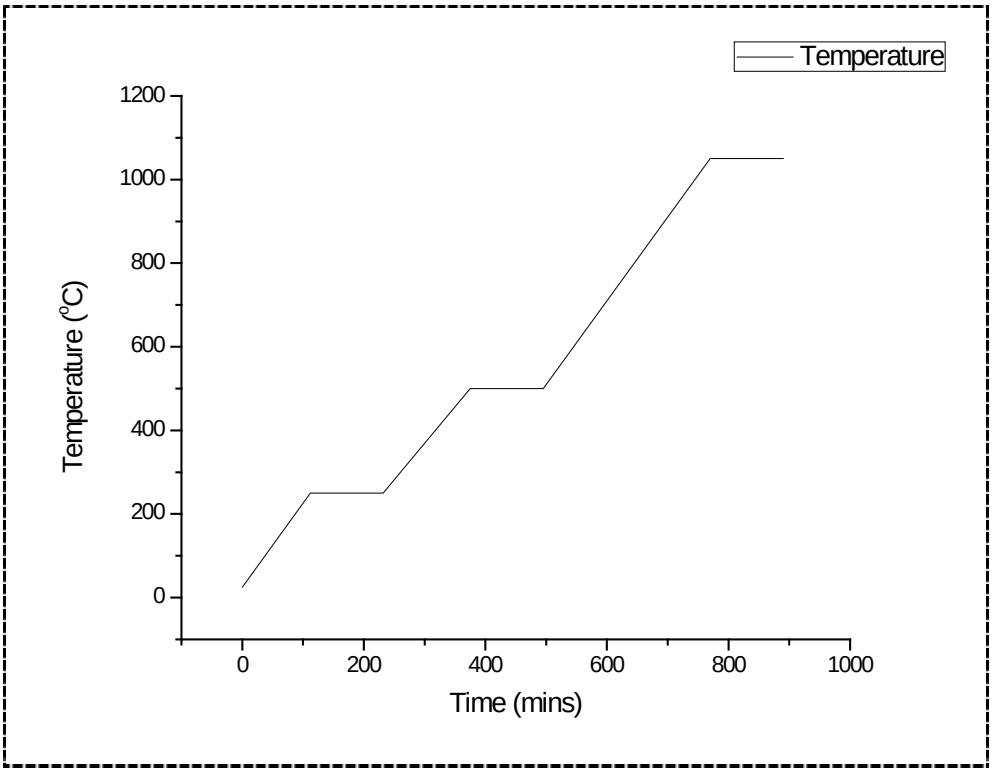

Fig 3.1.7: Sintering profile of the samples

a) The first holding temperature is 250^{o}C for 2hrs for complete removal of Naphthalene (boiling point is 218 ^{o}C).

b) The second holding temperature is at 500 ^{o}C for 2hrs for binder burn off. PVA decreases by 90% at 400 ^{o}C.

c) The final holding temperature is at 1050 ^{o}C for 2 hrs for viscous sintering to take place.

d) The rate of heating is maintained at 2 ^{o}C/min in order to avoid cracking of the porous material.

3.1.6 Preparation of SBF:

SBF was prepared using a novel method invented by A. Cuneyt Tas[12] as it resulted in a composition in closer proximity with that of Human plasma with respect to the concentration of Cl^- ions as compared to the Classical SBF composition proposed by Kokubo [13]. The relative compositions have been shown in table 3.1.2.

Ion	Kokubo's method	A. Cuneyt Tas' method	Human Plasma
Na^+	142.0	142.0	142.0
Cl^-	147.8	125.0	103.0
HCO_3^-	4.2	4.2	4.2
K^+	5.0	5.0	5.0
Mg^{2+}	1.5	1.5	1.5
Ca^{2+}	2.5	2.5	2.5
HPO_4^{2-}	1.0	1.0	1.0
SO_4^{2-}	0.5	0.5	0.5

Table 3.1.2: Comparative Ion concentrations of SBF and Human Plasma.

Order	Reagent	Amount(gpl)
1	NaCl	6.547
2	$NaHCO_3$	2.268
3	KCl	0.373
4	$Na_2HPO_4.\ 2H_2O$	0.178
5	$MgCl_2.\ 6H_2O$	0.305
6	$CaCl_2.\ 2H_2O$	0.368
7	Na_2SO_4	0.071
8	$(CH_2OH)_3CNH_2$	6.057

Table 3.1.3: Batch composition of SBF.

1. The preparation of SBF was done in a Teflon beaker as it is a saturated solution and crystallizes on the surface of glass.
2. The pH meter was calibrated using buffer solutions having pH 4 and 7.
3. The temperature is maintained at 37.4^{o}C throughout the process.
4. SBF solution was made by dissolving appropriate quantities of the mentioned chemicals in the proper order(as shown in table 3.1.3) in 700ml of DI water. A total of 40ml of 1M HCl is consumed for pH adjustments in the whole process. A 15ml aliquot is added just before the addition of the 6th reagent. Otherwise the solution will display slight turbidity. The remaining amount of HCl was used during subsequent titrations for making the pH 7.4. During the addition of 8th reagent, 260ml of additional water is used up.
5. The solution was then transferred into a pre-cleaned plastic bottle and stored at at a temperature below 10^{o}C.
6. The samples were then immersed in SBF for 1, 3, and 7 days, taken in a plastic container.

3.2 Characterization work

3.2.1 DSC/TG analysis:

Differential Scanning Calorimeter (DSC) shows thermal transformation behavior of the sample. When the sample undergoes any transformation, it either absorbs energy (endothermic) or releases it (exothermic). Similarly, Thermo Gravimetric Analysis (TGA) is the study of mass change of a sample as a function of temperature. This technique is useful for transformation involving absorption or release of gases from a sample containing condensed phase. The DSC/ TG characterization of the dried gel derived powder was conducted in a Netzsch 449C Thermal Analyser. This was done to identify the temperatures of the different reactions taking place, which can give us information about optimising the calcination temperature, crystallization temperature etc. The sample was heated in flowing Argon gas atmosphere at a heating rate of 10ºC/min. The weight loss measurements were also done in the same instrument and both the graphs were merged into one for comparative analysis.

3.2.2 XRD Analysis:

The X-ray diffraction analysis was done after heating the sample for 2hrs at a rate of 5^0C/min. to 3 different temperatures- 700ºC, 900ºC and 1200ºC for the analysis of the bioactive phase formed and also to study the evolution of phase with increase in temperature. Also the sample pellet immersed in SBF for a period of 7 days was analysed by XRD analysis for the formation of Hydroxy Carbonated Apatite (HCA) formation. The XRD characterization was done by Philips' X-ray diffractometer with Nickel filtered Cu Kα radiation (1.5406Aº). Generator Settings was 30 kV, 20 mA

The diffraction was done in the range of 10^o-60º of two theta value with scanning speed 0.04º/sec. The X-ray characterization was continuous type.

3.2.3 BET analysis:

BET of the samples before and after milling were done in order to find their particle size. Liquid Nitrogen was used as the sourse on Nitrogen gas. The surface area in a BET is found using the vol. of gas adsorbed on the surface of a material and relating it with the fall in pressure. The particle size can then be calculated from the surface area data.

3.2.4 Dilatometry:

Dilatometry of the sample with 0% Napthalene was done, to study the sintering behaviour of the composition. The heating rate was maintained at 10^{o}C/min. A horizontal dilatometer(NETZSCH DL 420) was used.

3.2.5 Bulk density, and Apparent porosity:

To measure bulk density and apparent porosity of the samples, first the Dry weight of the pellets was measured. Then they were immersed in a beaker containing kerosene and evacuated using a vacuum pump and desiccator till air bubbles stopped coming out. After that they were kept inside vacuum for 1 more hour. After removing from vacuum the suspended weight of the pellets was calculated and the soaked weight of the samples were calculated after cleaning off the surface from dripping kerosene with a moist tissue paper. To obtain bulk density (B.D.) the following formula was used:

B.D. = (dry weight)*(0.79)/(soaked weight-suspended weight)

To obtain apparent porosity (A.P.) in % the formula used is:

A.P. = [(soak weight-dry weight)*100/(soaked weight-suspended weight)] %

3.2.6 Linear Shrinkage:

The initial diameter is measured for the green body after pressing is done, and the final diameter is measured for the sintered sample.

The linear shrinkage(%) of the samples can be found by using the formula:

L.S.= [(initial diameter-final diameter)*100/initial diameter] %

3.2.7 Cold Crushing Strength:

The CCS is found using Tinius Olsen Materials Testing Machine (HK10S model). The pellets are in a horizontal position and force is applied on the top surface. The CCS value is found by dividing the top view(circular) surface area from the load at which the first fracture occurs, which is characterized by the first fall in the force-elongation graph.

$$CCS = F/(\pi * r * r)$$

Where F is the load and r is the radius of the pellet.

3.2.8 Bi-axial flexural Strength:

The Biaxial Tensile Strength of the pellets were measured by breaking the samples in a Tinius Olsen Materials Testing Machine (HK10S model) was used. It has a maximum load cell capacity of 10 KN. The biaxial tensile strength, S was obtained using the formula:

$$S = (2*P)/(\Pi * D * t)$$

where P =Maximum Load

D= Diameter of the pellet

t=Thickness of the pellet

3.2.9 Porosimetry:

A mercury porosimeter was used to find the pore size distribution of samples 0p,30p, and 50p. The sample underwent through both low pressure as well as high pressure mercury intrusion.

3.2.10 Optical microscope Imaging:

The porous samples of uniform porosity distribution as well as the samples having radially graded porosity were viewed under an optical microscope. The images were taken using Olympus optical microscope fitted with a CCTV camera using Image analysis software. While taking the photographs focus was laid on the pore size; pore distribution; and the gradient of porosity. The pellets were placed on a slide and then viewed through the monitor screen.

3.2.11 Scanning Electron Microscopy(SEM) Imaging:

Microstructure of the HCA covered pellets immersed in SBF for 1day, 3days, and 7days were seen under SEM(JOEL-JSM 6480LV) using back scattered electron mode to study the growth of HCA with time, so as to verify the bioactivity of the material. The generator voltage was set at 15kV and the magnification was 200X. The pellets were washed in isopropyl alcohol. The samples were electroplated with platinum for making the surface conducting.

3.2.12 Energy-dispersive X-ray(EDX) spectroscopy:

The EDX of the HCA was done to check the incorporation of $(CO_3)^{2-}$ ions for the satisfaction of the bioactivity criteria of the material. The EDX is done over a small surface area showing only the HCA.

3.2.13 Fourier Transformed Infrared Spectroscopy (FT-IR):

The FTIR(Perkin Elmer US) analysis for studying the presence of different functional groups in the SBF immersed pellets with duration of 1day, 3days, and 7 days was done. The FTIR spectra were taken of the powder sample by scrapping off the surface of the pellets. The samples were pressed to a circular disc (diameter 10 mm) by mixing with KBr, keeping the KBr: Sample weight ratio 20:1. The samples were scanned in the wave number range 4000-400 cm^{-1}.

CHAPTER 4:
RESULT AND DISCUSSION

4.1 Optimization of sintering temperature and profile:

The sintering temperature of the pellets was optimised by sintering the samples at different temperatures.

- At first the samples were sintered at 1000^{o}C for 2hrs. It was observed that the samples showed very low mechanical strength due to incomplete sintering. As the sample consists of a large amount of glassy phase, it follows a viscous sintering mechanism which essentially comprises of the formation of glassy melt which fills the pores and causes densification and shrinkage due the capillary force arising due to the covering of the grains of the crystalline phase by the glassy melt.
- So the next firing was done at 1300 ^{o}C. It was seen that the pellets completely melted at this temperature. This low melting point of the material can be explained by the high Na_2O (23.8 wt%) content of the sample.
- The next sintering was done at 1100 ^{o}C. Though the samples did not melt, but it showed a considerable shrinkage and deformation. As porosity requirement of the samples cannot be fulfilled with such high shrinkage and also the shape stability could not be compromised.
- So finally the sintering temperature was set at 1050 ^{o}C. This temperature gave very good results. There was no deformity in the structure and also the shrinkage was not very high.
- The sintering time was kept at 2hrs as this gave satisfactory results.

4.2 **DSC/TG analysis:**

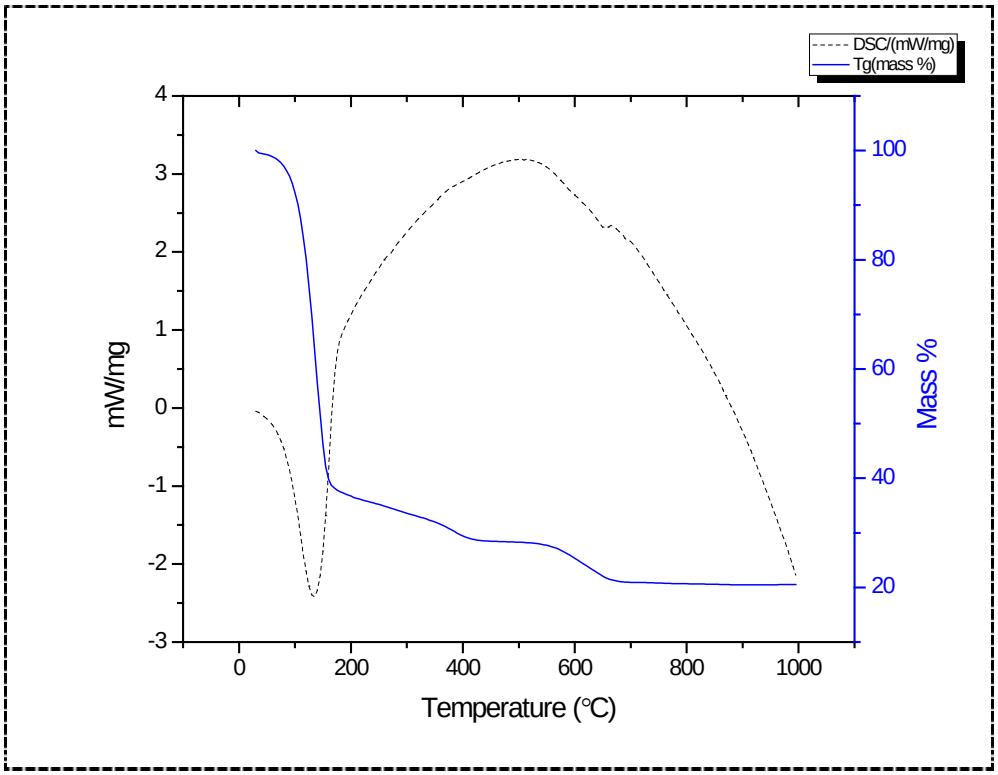

Fig 4.1: DSC-TG plot of the sample

1. The initial weight loss in TG plot and the endothermic peak in DSC plot at 133^{o}C is due to the initial loss of water from the sample.
2. Another fall in weight before 400 ^{o}C is due to the decomposition and evaporation of the chemically bounded water from the sample.
3. The fall in weight from 550 ^{o}C to 650^{o}C is due to the decomposition of $Ca(NO_3)$ and $NaNO_3$ into respective oxides with evolution of Nitrogen dioxide gas.
4. The endothermic peak in DSC plot at 650 ^{o}C is due to the decomposition of $NaNO_3$.
5. The exothermic peak at 510 ^{o}C is due to the crystallization of $Na_4Ca_4Si_6O_{18}$.
6. From the TG graph it can be seen that the weight becomes constant after 650 ^{o}C, marking the end of all the decomposition reactions. Thus the calcination of the sample was done at 700 ^{o}C, leaving a margin of 50 ^{o}C to account for the errors in the furnace thermometry.

4.3 XRD Analysis:

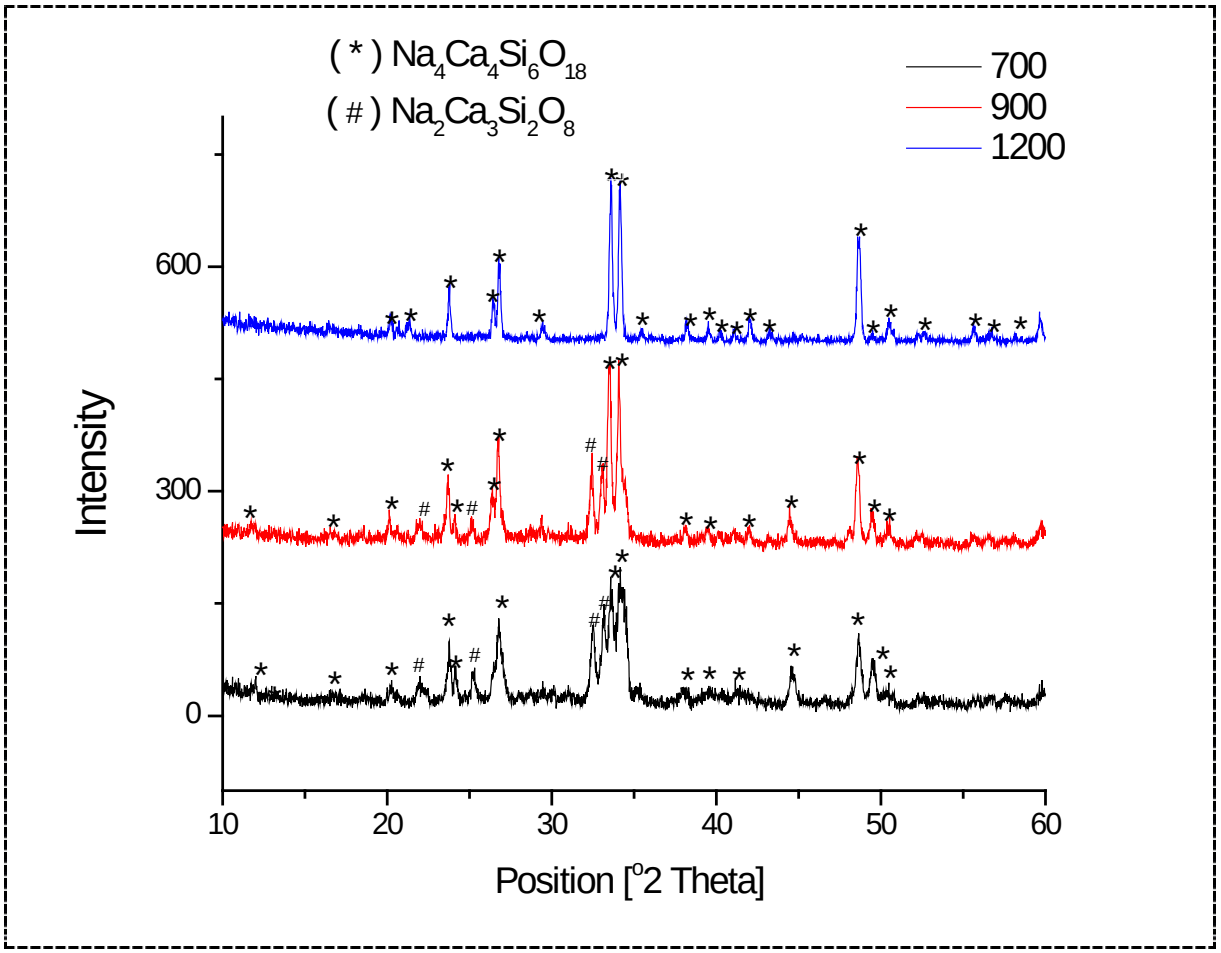

Fig. 4.2: XRD plot of the samples heat treated at 700°C, 900 °C, and 1200 °C

1. The comparative XRD analysis (as shown in fig 4.2) shows the formation of two crystalline phases $Na_4Ca_4Si_6O_{18}$ and $Na_2Ca_3Si_2O_8$ after calcination at 700°C (bottom graph).
2. The former phase has been documented to be a bioactive phase.[10]
3. The height of the peaks increases as the temperature increases. Also the width of the peaks increases with increase in temperature showing the growth in crystallite size.
4. In the XRD at 1200°C (top graph), it can be seen that there is no $Na_2Ca_3Si_2O_8$ phase due to its vitrification.

5. The $Na_2Ca_3Si_2O_8$ phase is bio-inert in nature and does not add to bioactivity but does help in increasing the strength of the material due to its crystalline nature.

Pos. [°2Th.]	Height [cts]	FWHM [°2Th.]	d-spacing [Å]	Rel. Int. [%]
20.2030	25.10	0.1574	4.39549	13.05
20.6174	8.58	0.2362	4.30807	4.46
21.3691	22.91	0.1181	4.15821	11.91
23.7554	67.02	0.1181	3.74563	34.86
26.4380	48.62	0.1574	3.37134	25.29
26.7571	102.63	0.0590	3.33185	53.38
29.4158	15.16	0.2755	3.03649	7.88
33.6113	192.27	0.1181	2.66644	100.00
34.1886	185.25	0.1574	2.62273	96.35
35.4625	10.10	0.2362	2.53137	5.25
38.1743	21.29	0.1968	2.35757	11.07
39.5028	19.95	0.1181	2.28128	10.37
40.2480	10.39	0.2362	2.24075	5.40
41.1023	14.09	0.1378	2.19613	7.33
42.0393	29.53	0.1968	2.14932	15.36
43.2821	9.60	0.2362	2.09045	4.99
45.3512	3.37	0.9446	1.99977	1.75
48.5905	139.35	0.0984	1.87376	72.48
49.4747	8.05	0.2362	1.84232	4.18
50.4198	19.76	0.2362	1.80999	10.28
52.4720	6.84	0.6298	1.74393	3.56
55.6426	20.01	0.1968	1.65184	10.41
56.6342	8.03	0.3936	1.62525	4.18
58.1465	5.47	0.2400	1.58521	2.85

Table 4.1: Peak list of the matching peaks at 1200°C for $Na_4Ca_4Si_6O_{18}$ phase.

6. The crystallite size of the $Na_4Ca_4Si_6O_{18}$ phase can be found by using the **Scherrer** formula:

$$D_p = (0.94*\lambda)/(\beta_{1/2}*\text{Cos}\ \theta)$$

Taking

$\lambda = 1.5406\ 10^{-10}$ mtr. $\beta_{1/2} = 0.1181° * \pi/180$ $\theta = 33.6113/2$

D_p = 73.3916 nm.

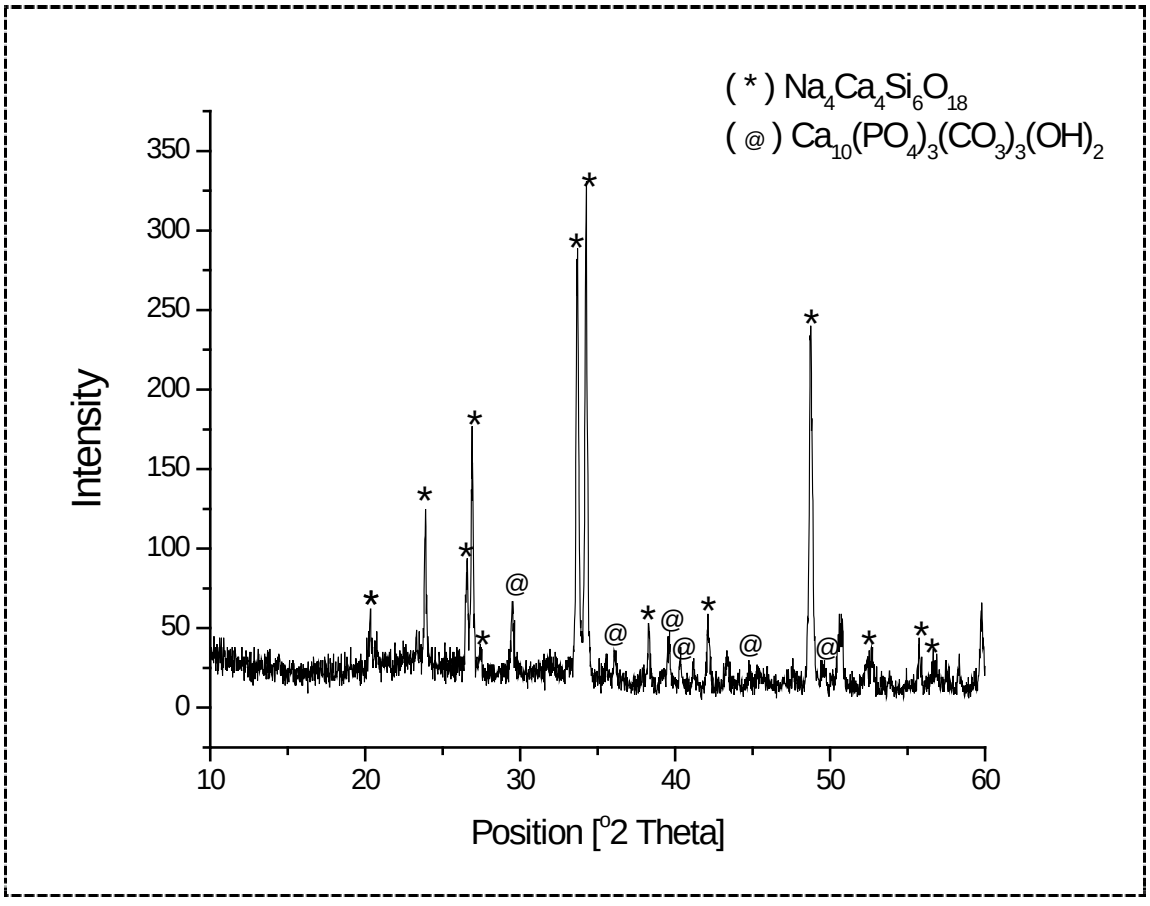

Fig. 4.3 XRD plot of the samples immersed in SBF for 7 days.

7. The small peaks of $Ca_{10}(PO_4)_3(CO_3)_3(OH)_2$ in the fig 4.3 conforms the formation of HCA layer over the material.

4.4 BET Analysis:

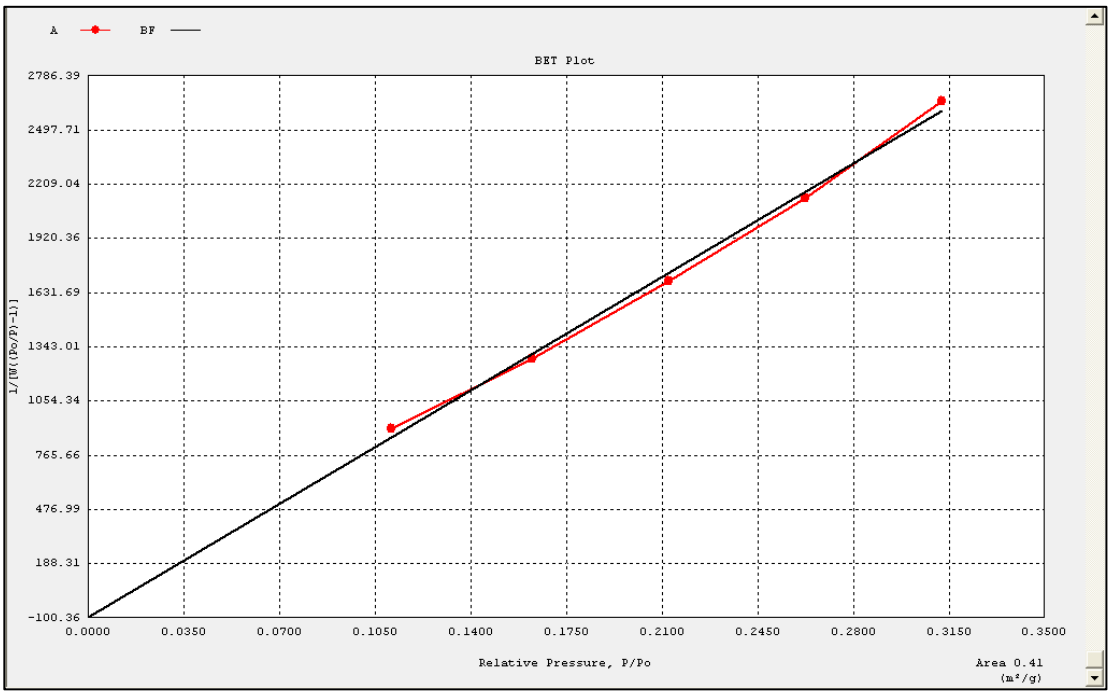

(a)

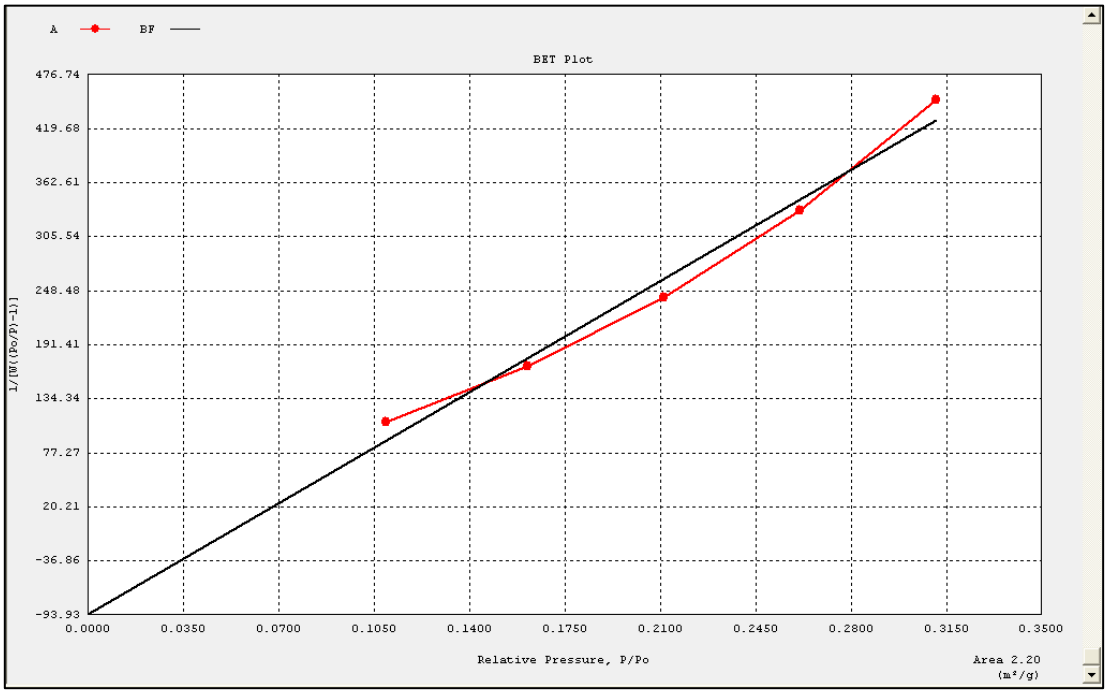

(b)

Fig 4.4: BET Isotherms of powder samples before (a) and after (b) ball milling.

1. From fig 4.4, we can see that there is a increase in surface area of the particles from 0.41(0.4083 from BET summery) m^2/gm to 2.20(2.199 from BET summery) m^2/gm on ball milling for 6 hrs.
2. The particle size can be calculated from the surface area data using the formula:

   Particle diameter= 6/(bulk density*Surface area)

   Using this formula and taking BD to be 2.65gm/cc; the particle size was found to be 5.545µm before milling and 1.030µm after milling.

4.5 Dilatometry:

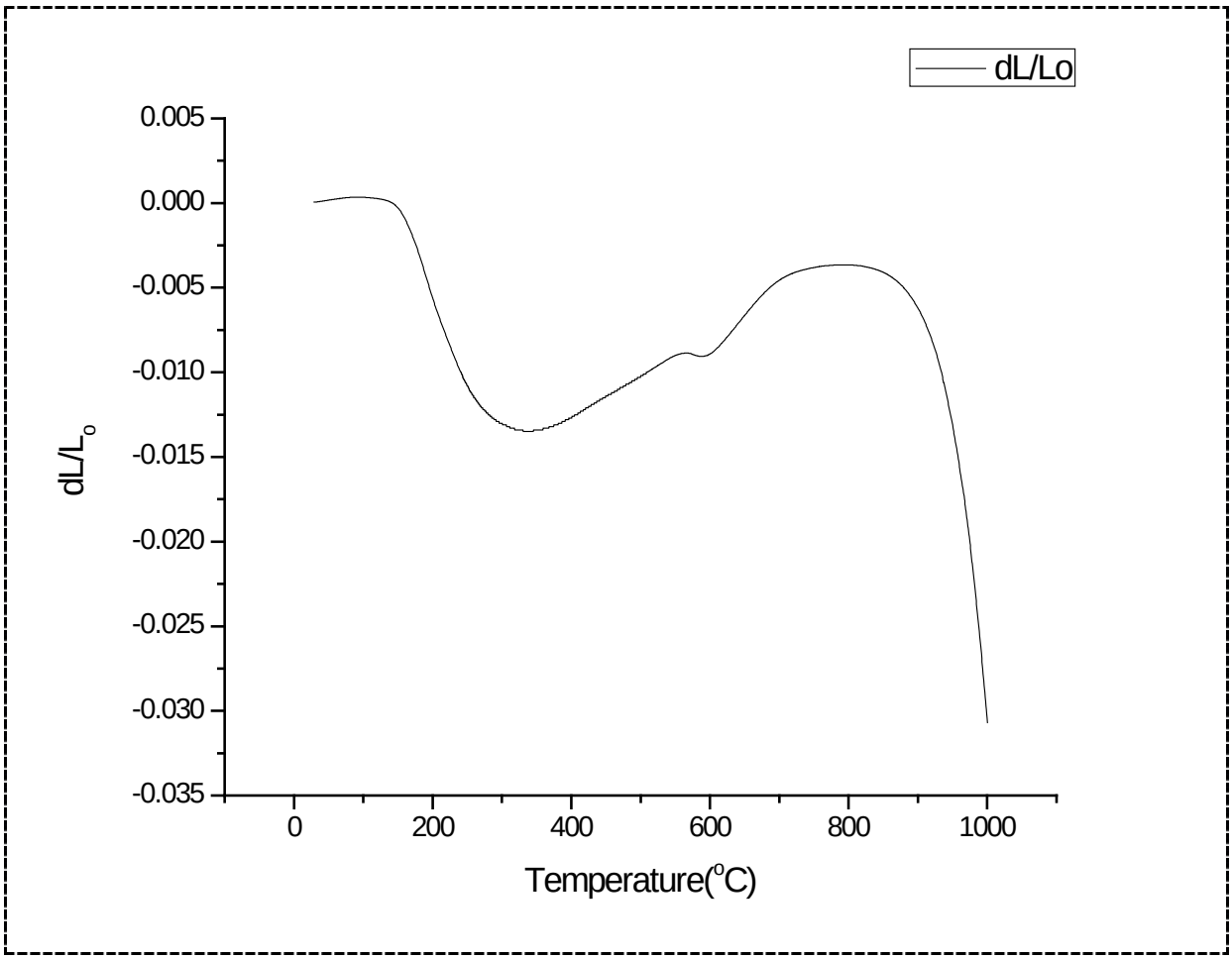

Fig 4.5: Dilatometry plot of 0p sample.

From the Dilatometry plot in the fig 4.5 it can be observed that:

1. There are two major shrinkages in the sample. The first one ranging from 100^{o}C-300 ^{o}C, and another from 900 ^{o}C onwards. The reason for the 1st shrinkage which accounts for 1.5% shrinkage can be due to the sudden binder and moisture burn off, while the 2nd shrinkage may be due to the starting of the formation of liquid phase and the onset of viscous sintering.
2. The first glass transition temperature occours at 560 ^{o}C, and is marked by a positive peak.
3. Crystallization occours at 590 ^{o}C and is marked by a decrease in length.
4. The second glass transition temperature starts at around 700 ^{o}C leading to crystallization of the remaining glassy phase at 850 ^{o}C.

4.6 Bulk Density:

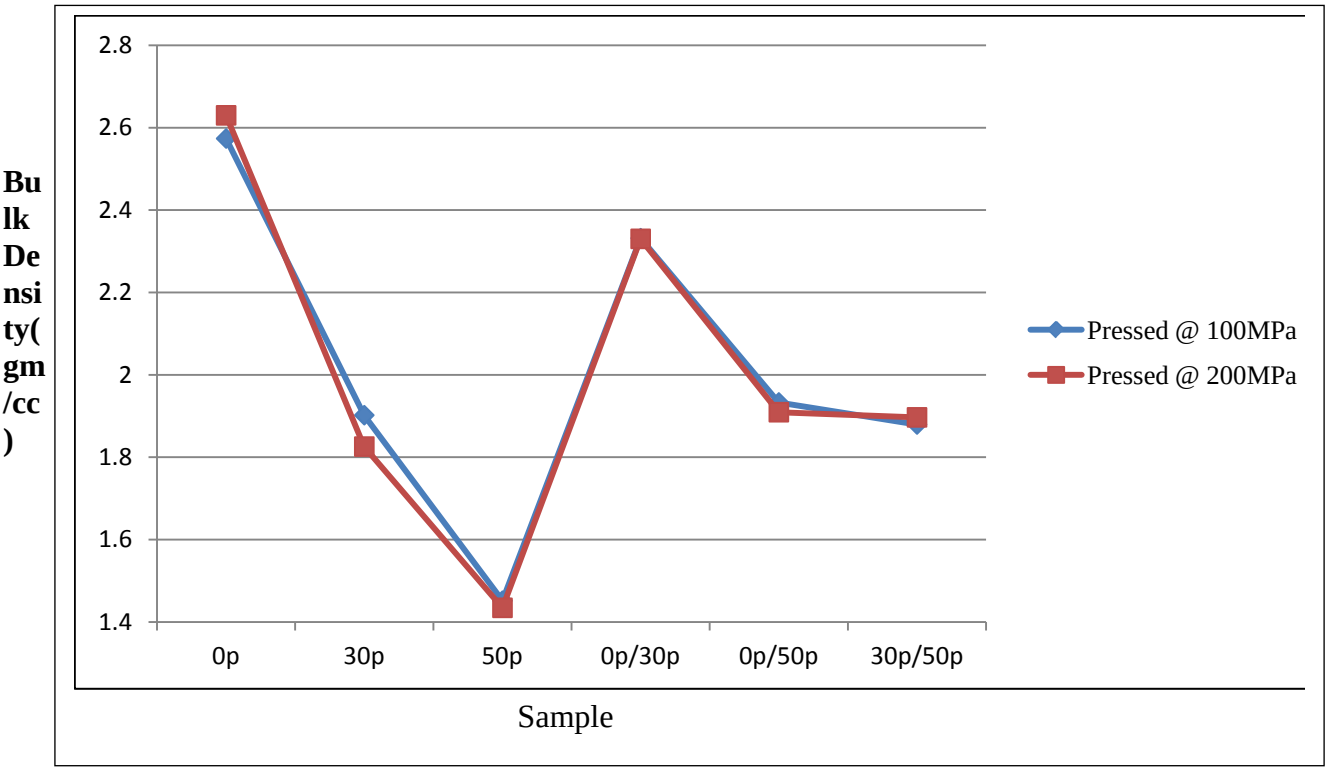

Fig 4.6: Bulk Density of the samples.

Sample name	Bulk density(gm/cc)	Bulk density(gm/cc)
	Pressed @ 100MPa	Pressed @ 200MPa
0p	2.573	2.629
30p	1.901	1.825
50p	1.451	1.434
0p/30p	2.331	2.330
0p/50p	1.932	1.909
30p/50p	1.879	1.896

Table 4.2: Bulk Density of samples.

From the fig 4.6 it can be observed that there was a very small increase in the Bulk density of the samples on increasing the pressure from 100MPa to 200MPa. The value of the BD showed close resemblance to the theoretical values that can be calculated

using the law of mixtures. The Bulk density values decreased with increase in the weight percentage of naphthalene used.

4.7 Apparent porosity:

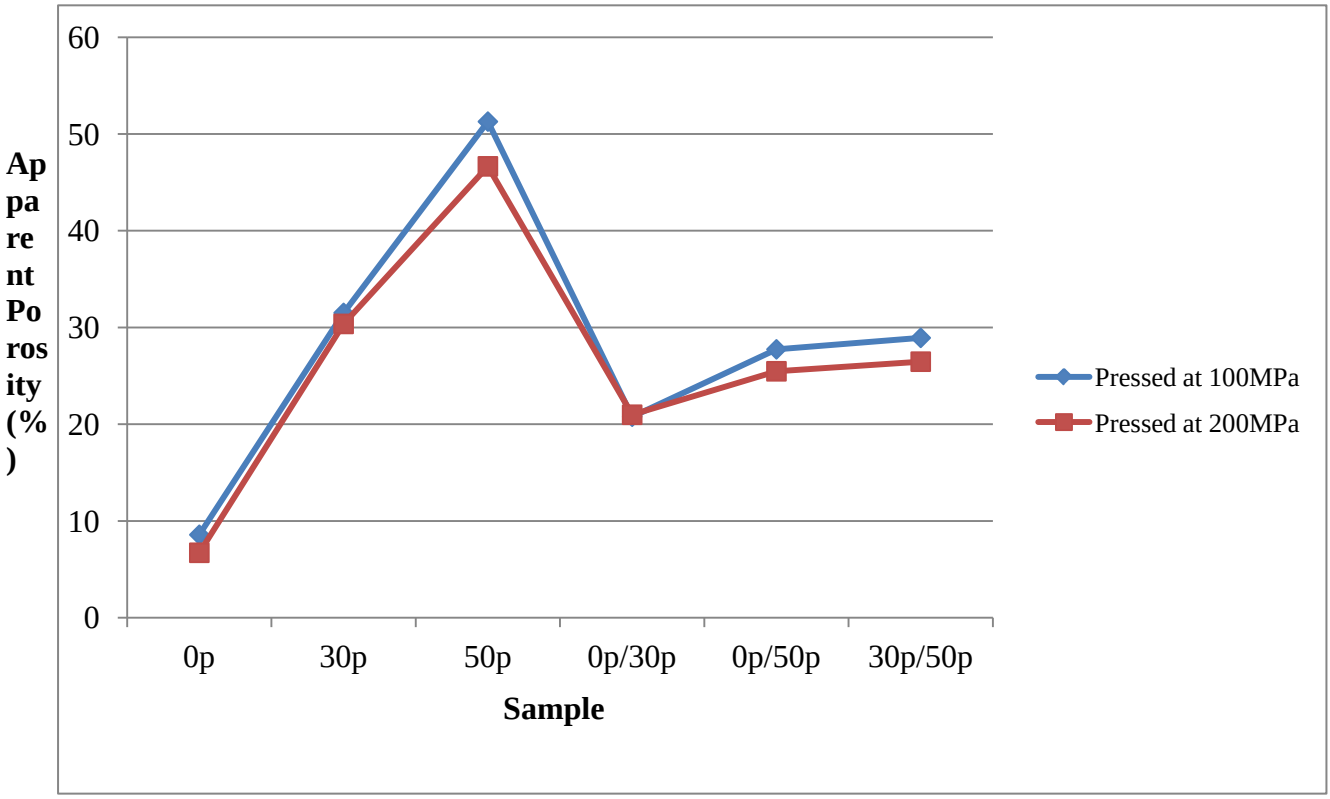

Fig. 4.7 Apparent porosity of samples.

Sample name	Apparent Porosity (%) Pressed @ 100MPa	Apparent Porosity (%) Pressed @ 200MPa
0p	8.574	6.710
30p	31.51	30.369
50p	51.284	46.658
0p/30p	20.776	20.981
0p/50p	27.742	25.473
30p/50p	28.928	26.466

Table 4.3: Apparent porosity of samples

From fig. 4.7 it can be noticed that the apparent porosity decreased with increase in pressing load. The value of the AP showed close resemblance to the theoretical values that can be calculated using the law of mixtures. There is a marked increase in AP values with increase in weight percentage of naphthalene used. So we may conclude that porosity as high as 50% can be achieved using naphthalene as pore former.

4.8 Linear Shrinkage:

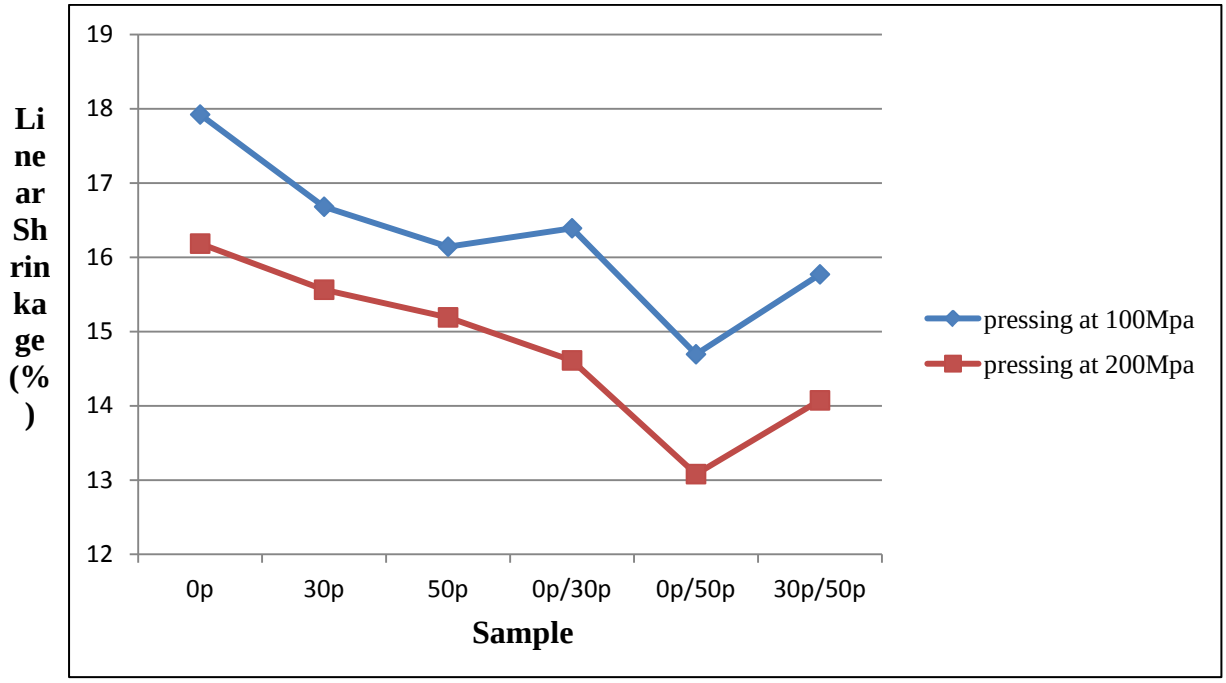

Fig 4.8: Linear Shrinkage of samples.

Sample name	Linear Shrinkage (%) Pressed @ 100MPa	Linear Shrinkage (%) Pressed @ 200MPa
0p	17.922	16.183
30p	16.680	15.562
50p	16.142	15.190
0p/30p	16.390	14.610
0p/50p	14.693	13.079
30p/50p	15.769	14.072

Table 4.4: Linear Shrinkage of samples.

From the fig 4.8 it was noticed that the Linear Shrinkage decreased with increase in pressing load. Which explains the decrease in Apparent porosity with increase in load. LS also decreased with increase in naphthalene content, though the effect was not very prominent.

4.9 Cold Crushing Strength:

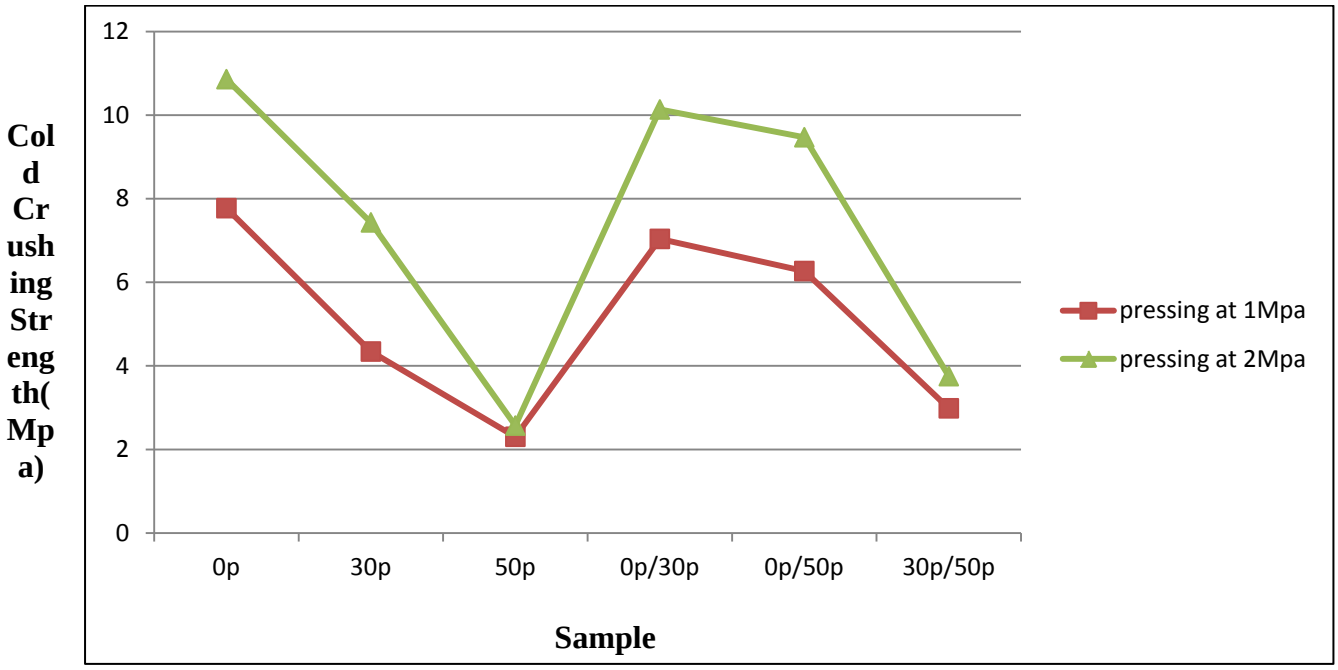

Fig. 4.9: CCS of samples.

Sample name	CCS(MPa) Pressed @ 100MPa	CCS(MPa) Pressed @ 200MPa
0p	7.774	10.861
30p	4.343	7.433
50p	2.303	2.571
0p/30p	7.038	10.136
0p/50p	6.269	9.471
30p/50p	2.984	3.754

Table 4.5: CCS of samples

From the fig. 4.9 it was noticed that the CCS value showed a great improvement with increase in pressing load except in the case of 50% naphthalene containing body, where not much improvement could be seen. The CCS value decreases with increase in the weight percentage of naphthalene used. The maximum CCS was found to be 10.9 for 0p and minimum was 2.6 for 50p samples in case of 200MPa pressing.

4.10 Bi-axial Flexural Strength (BFS):

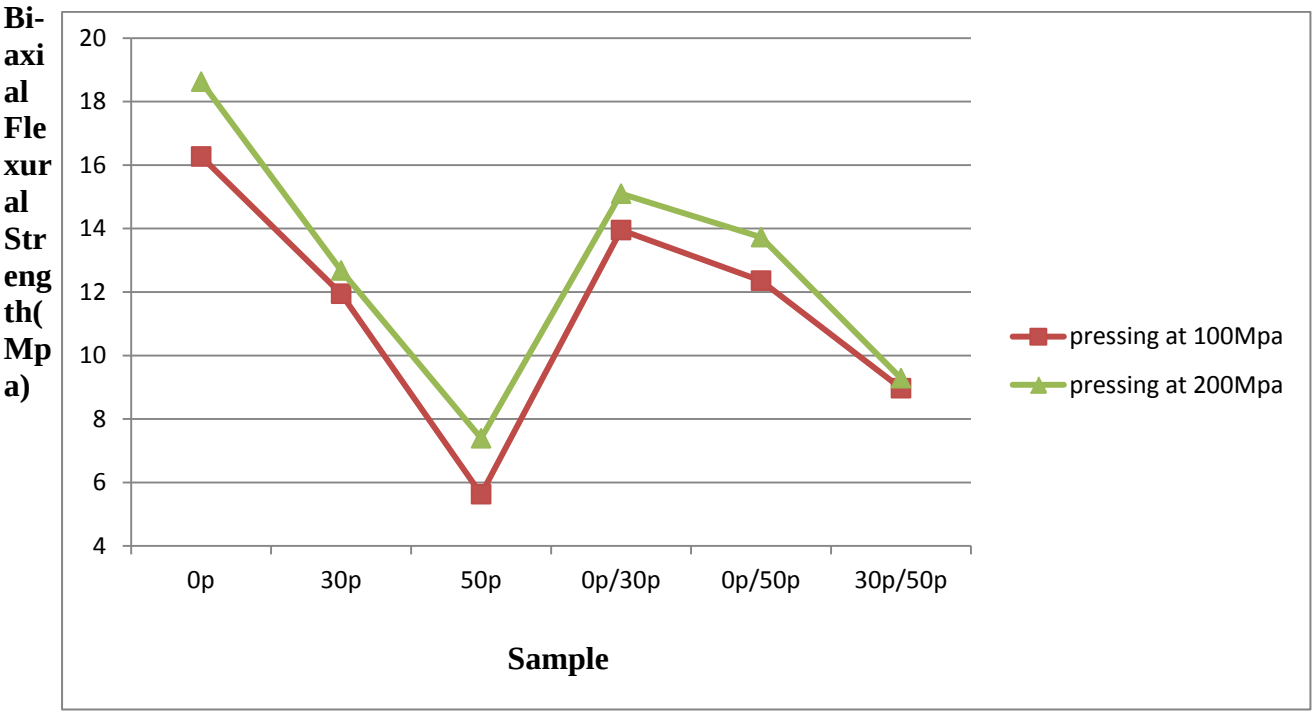

Fig. 4.10: Bi-axial flexural strength of samples.

Sample name	BFS(MPa)	BFS(MPa)
	Pressed @ 100MPa	**Pressed @ 200MPa**
0p	16.27	18.628
30p	11.946	12.678
50p	5.630	7.391
0p/30p	13.952	15.098
0p/50p	12.358	13.729
30p/50p	8.969	9.284

Table 4.6: Bi-axial flexural strength of samples.

From fig 4.10, it can be seen that the biaxial flexural strength showed an improvement of 1-2MPa on increasing the pressing load. Its value decreases with increase in porosity of the samples. A maximum value of 18.6MPa strength was obtained in case of 0p sample pressed at 200Mpa.

4.11 Porosimetry:

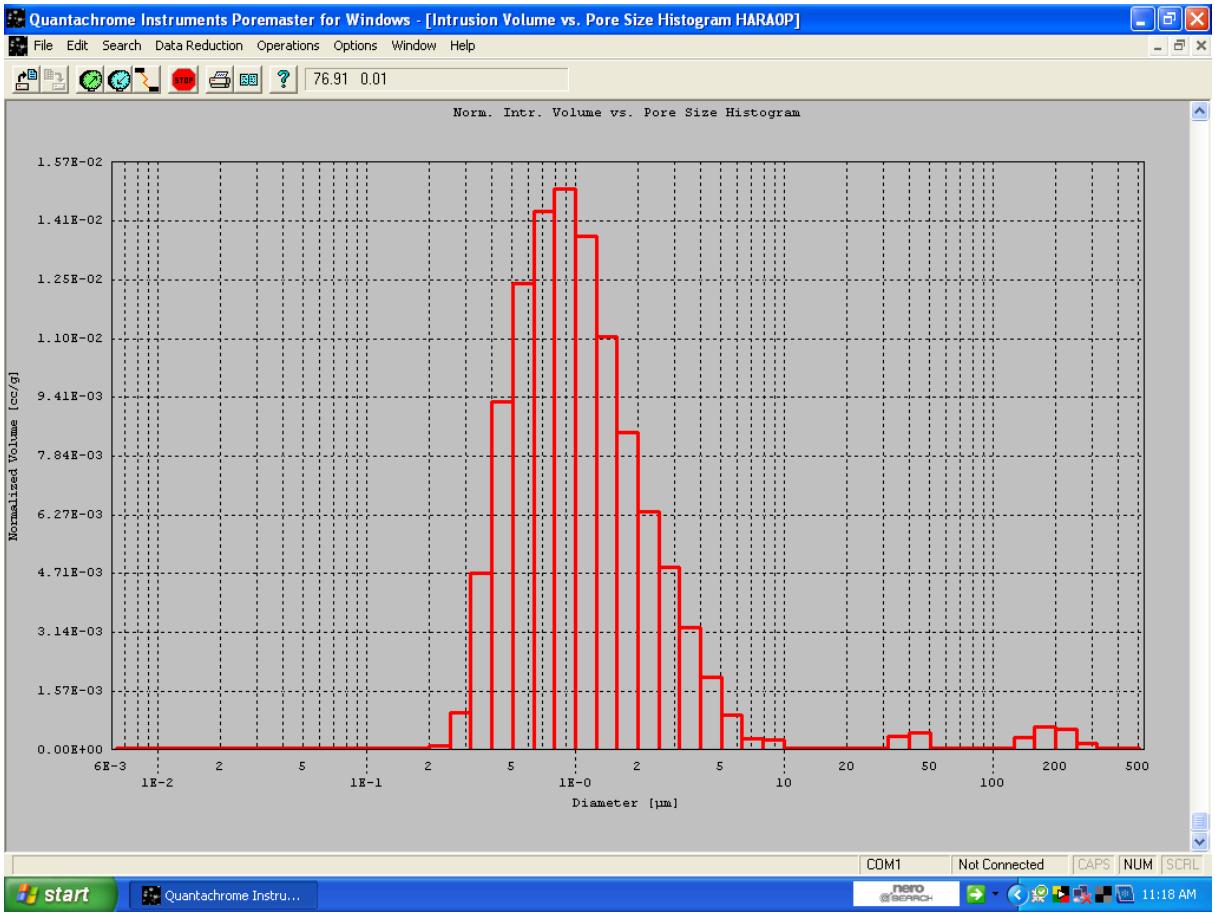

Fig 4.11: Normalized vol(cc/gm) vs diameter(micron) histogram for 0p sample.

From the fig 4.11 it can be observed that the maximum pore size distribution is for 1µm range. But still there is a small amount of pore size distribution in the range of 50µm and

200µm. So it can be assumed that 0p samples on itself cannot cause prominent angiogenesis, and needs to be blended with materials with higher porosity.

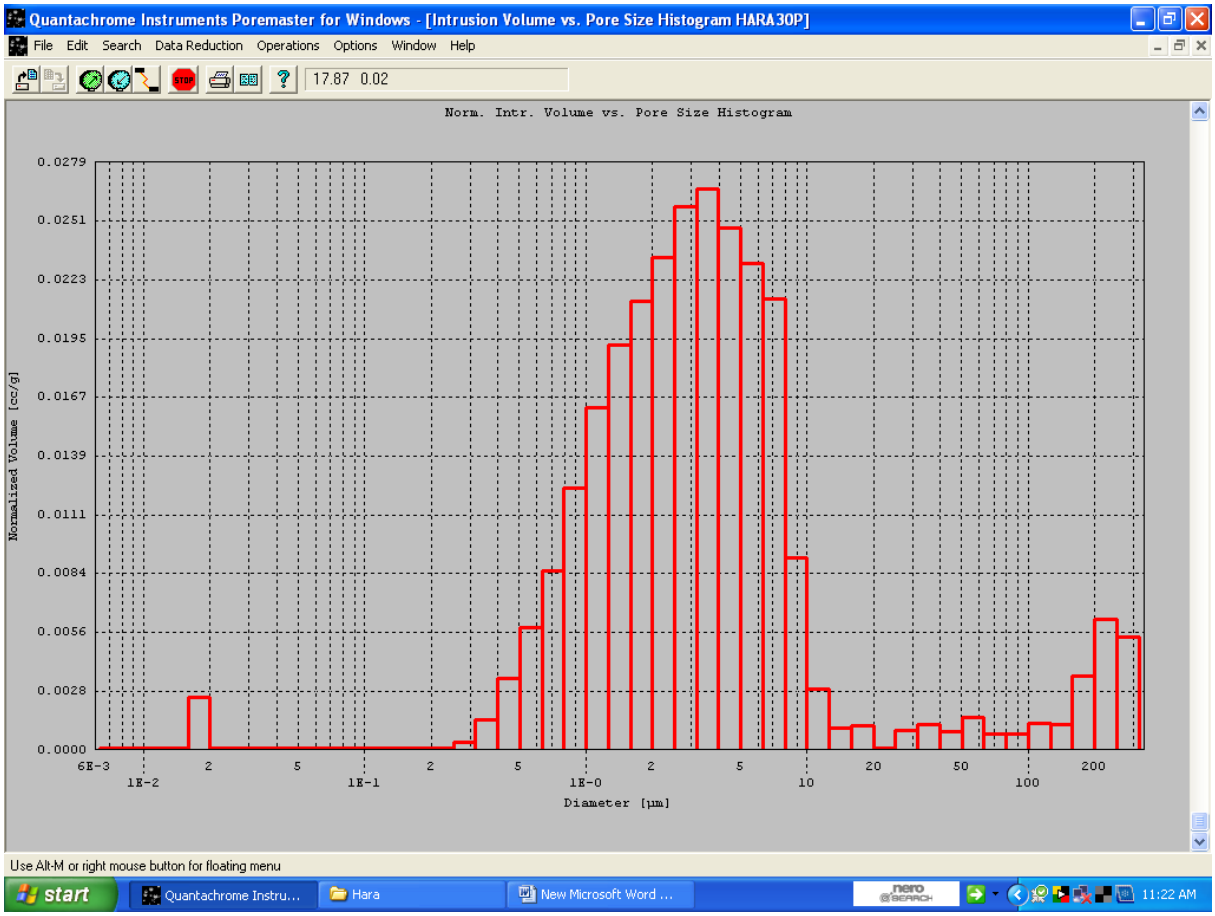

Fig 4.12: Normalized vol(cc/gm) vs diameter(micron) histogram for 30p sample.

Fig. 4.12 shows the pore size distribution histogram of 30p sample. From the graph it can be inferred that the maximum volume fraction of pores lie in the range of 0-10µm. there is also a considerable pore size in the range of 100- 200µm. The overall distribution function shows a positive deviation in respect to pore size as compared to the 0p sample. The pore size distribution shows a continuous pattern ranging from 0.2 µm to 200µm indicating the presence of pores of all the sizes.

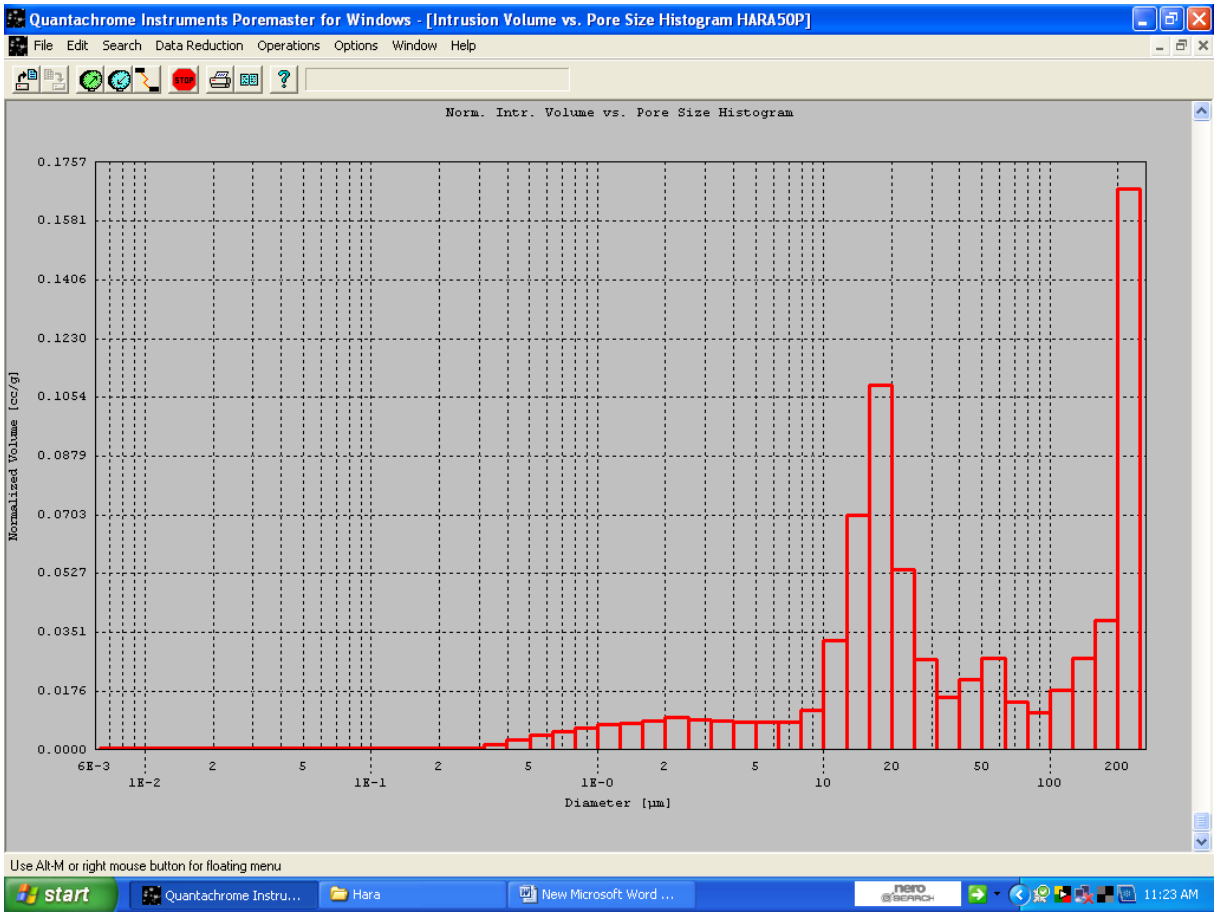

Fig 4.13: Normalized vol(cc/gm) vs diameter(micron) histogram for 50p sample.

Fig. 4.1 shows the pore size distribution histogram of 50p sample. From the graph it can be inferred that the maximum volume fraction of pores lie in the range of 100-200µm. there is also a considerable pore size in the range of 10- 50µm. The overall distribution function shows a positive deviation in respect to pore size as compared to the 0p and 30p samples. The pore size distribution shows a continuous pattern ranging from 0.2 µm to 200µm indicating the presence of pores of all the sizes. The large volume fraction of pores with size larger than 100µm indicates that this material can cause angiogenesis.

Important results from porosimetry analysis:

1. Pore size increases with increase in porosity due to increase in percolation of the pores.

2. There is an increase in the concentration of pores having size> 100 micron as we increase the porosity.
3. Sample containing 50% naphthalene showed considerable amount of >100 micron pores.
4. Presence of pores larger than 100 micron is essential for Angiogenesis.
5. Higher porosity means higher exposed surface area which leads to faster deposition rates.

4.12 Optical Microscopy:

(a) 0 porosity

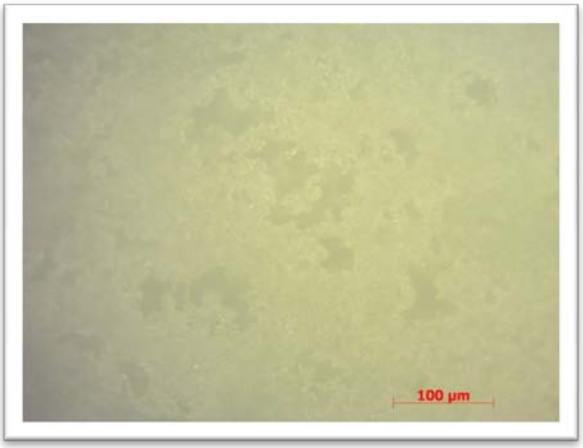

(b) 30 porosity

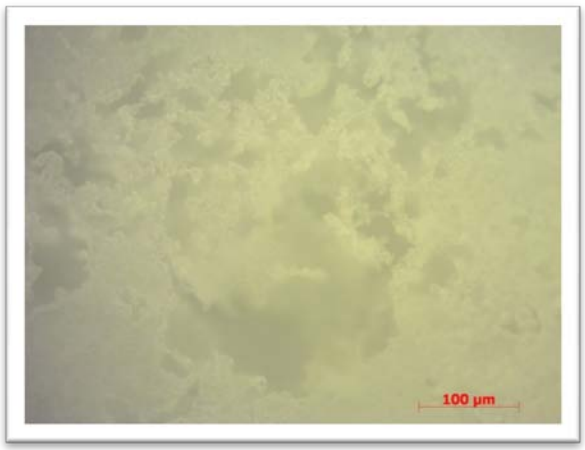

(c) 50 porosity

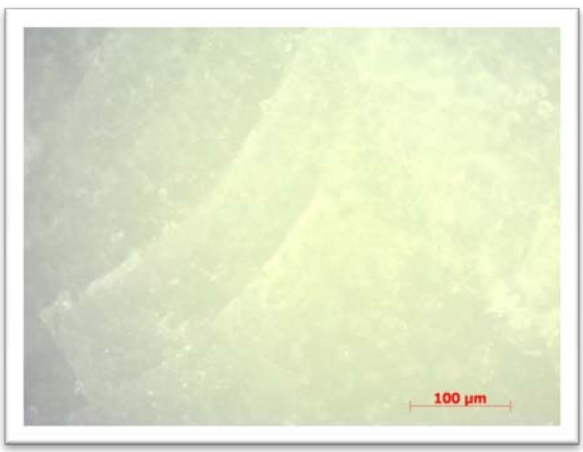

(d) 0 porosity/30 porosity

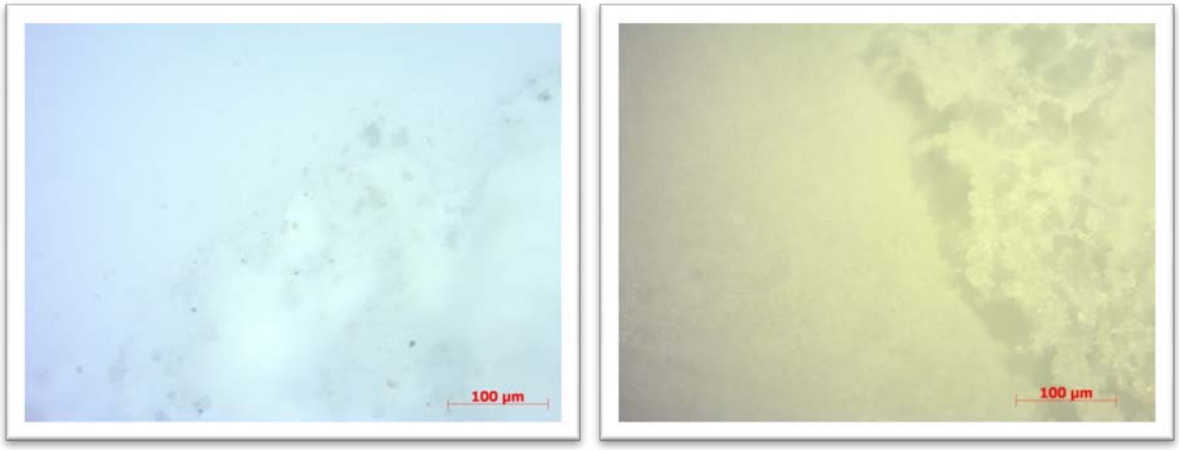

(e) 0 porosity/50 porosity (f) 30 porosity/50 porosity

Fig 4.14: Optical microscopy images of the samples.

1. From the optical microscopy graphs, the pore size, pore distribution can be easily seen. Except in case of samples with 0% Naphthalene, pores greater than the size of 100 micron can be seen.
2. In case of samples with 50% Naphthalene pores as large as 300 micron were observed.
3. In case of samples with porosity gradients, the part of the sample showing the transition of porosity has been shown in the photographs.
4. The uniformity in the distribution of pores was found to increase with the increase in the weight percentage of Naphthalene used.

4.13 Scanning Electron Microscopy (SEM):

1. From the SEM images in fig 4.15, the growth of HCA on the surface of the pellets is clearly visible.
2. From fig4.15 (a), (b) and (c) it can be seen that the density of surface covering with HCA was seen to increase proportionally with the time of immersion of the samples in SBF.

3. One of the images fig 4.15(d), was taken at 5000X for obtaining the EDX of the HCA coverage.

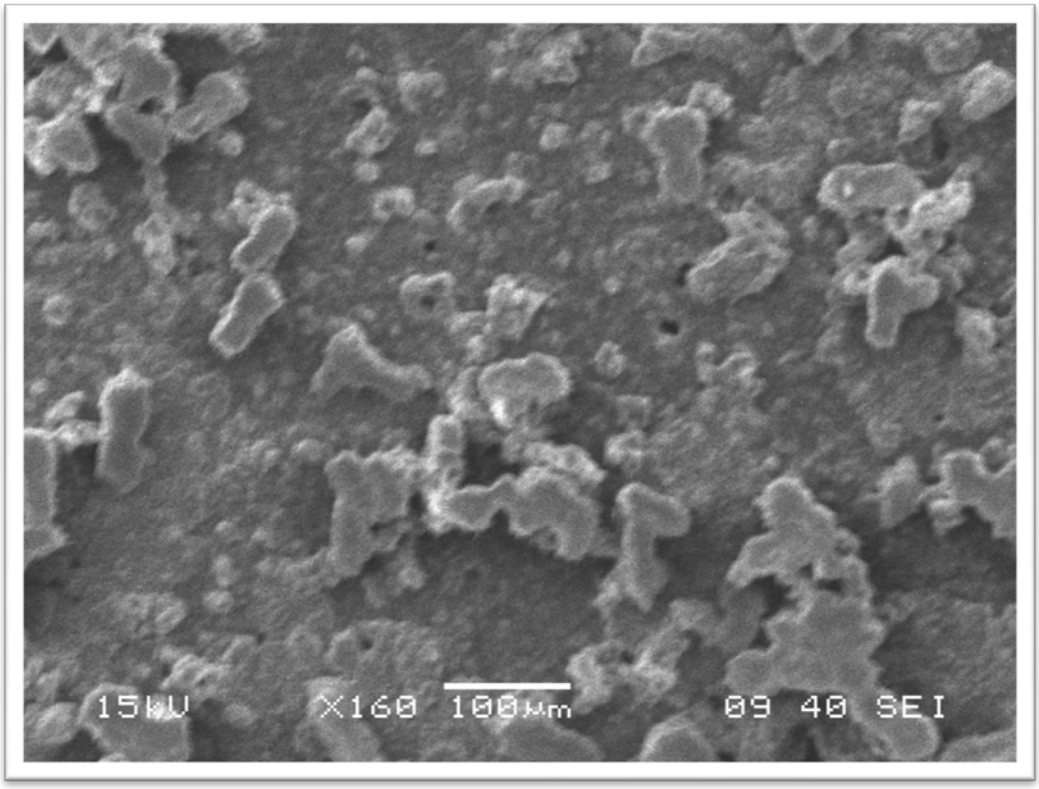

(a) Morphology of the surface of sample after 1 day in SBF

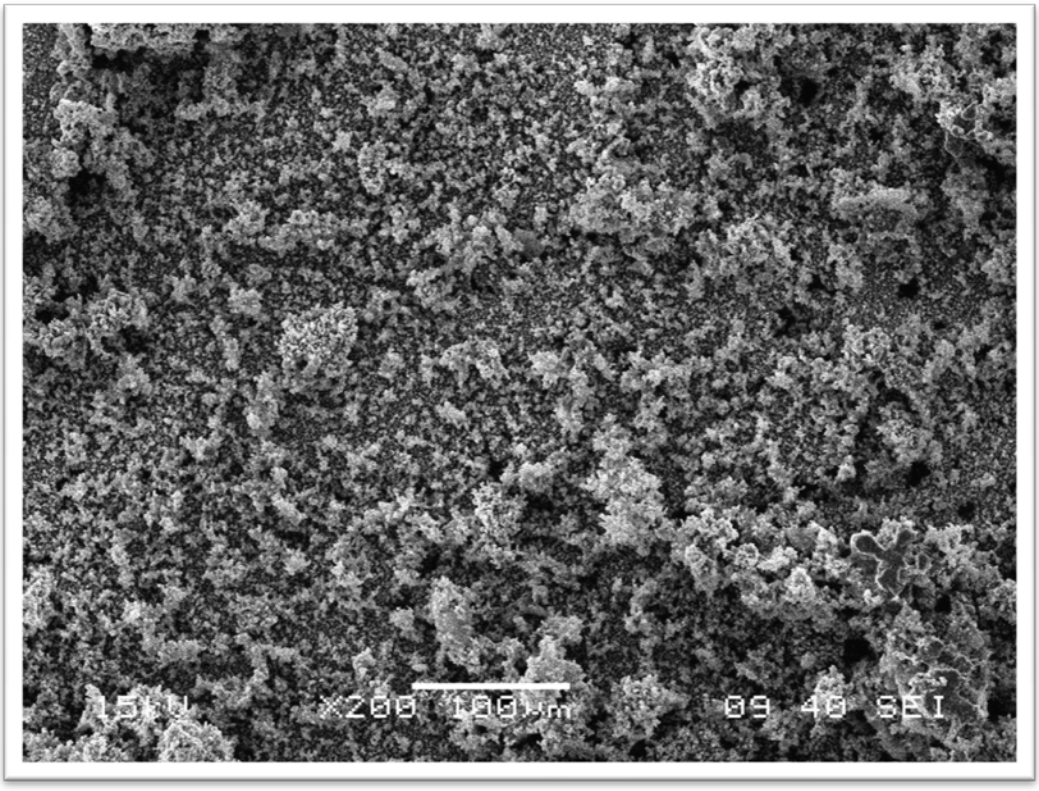

(b) Morphology of the surface of sample after 3 days in SBF

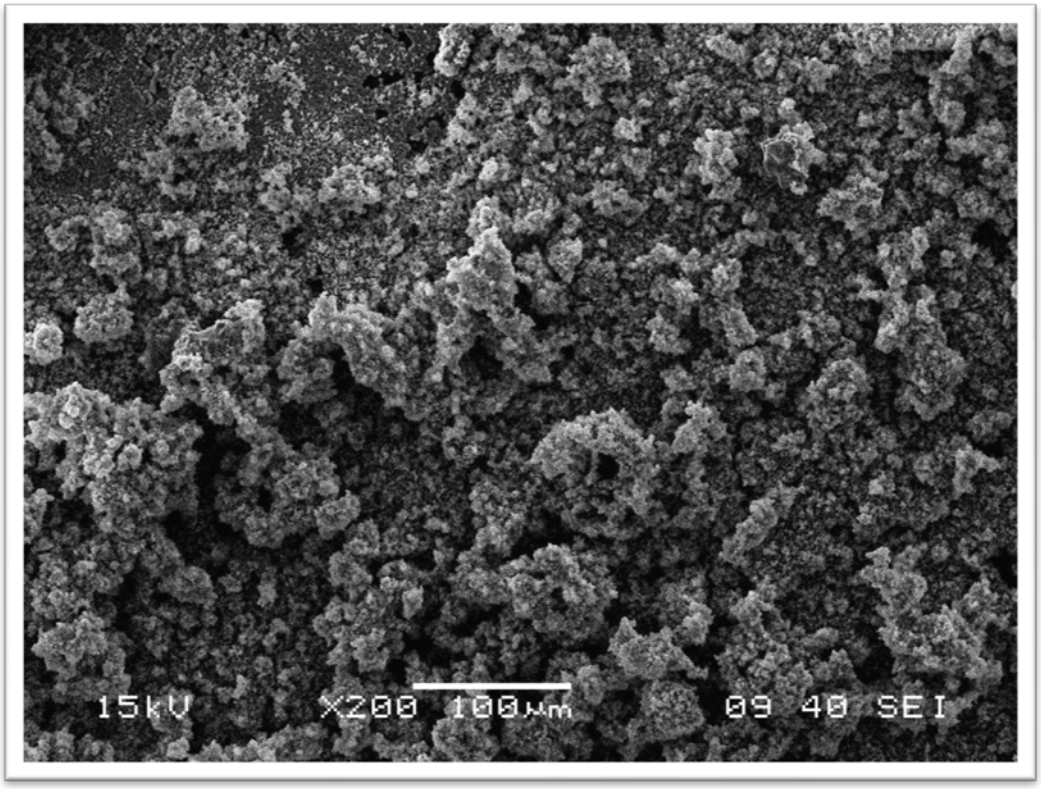

(c) Morphology of the surface of sample after 7 days in SBF

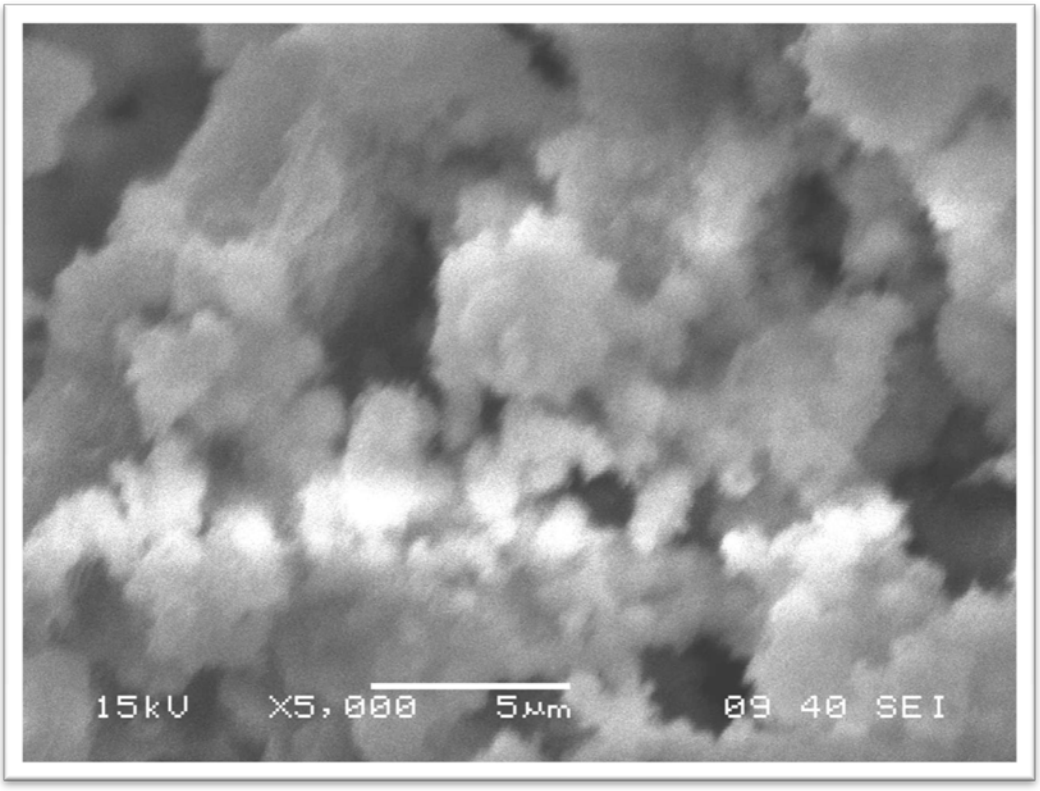

(d) Morphology of the HCA layer after 7 days in SBF at 5000X for EDX

Fig 4.15: SEM images of the samples immersed in SBF for1(a), 3(b), and 7(c) days. And (d) shows the microstructure of HCA layer

4.14 EDX:

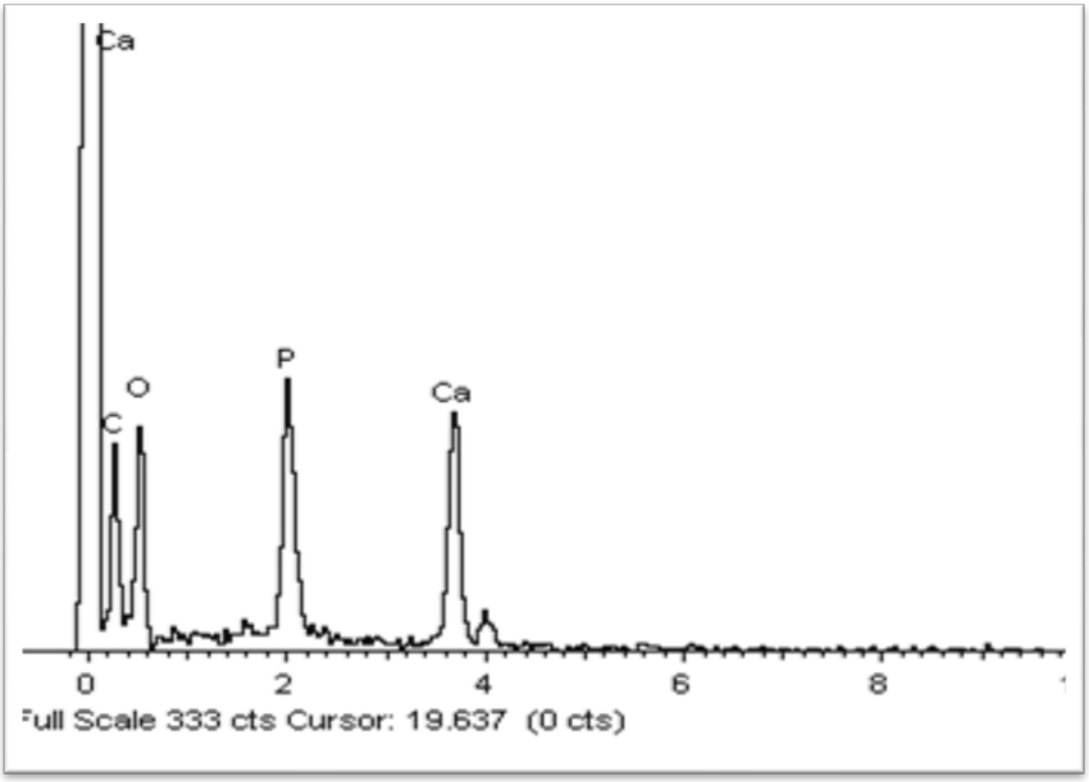

Fig 4.16:EDX showing formation of HCA

From the fig 4.16, we can observe the following:

1. The presence of the Carbon peak indicates the formation of HCA.
2. The Calcium and Phosphorous peaks indicate the growth of Amorphous Calcium Phosphate(ACP).

4.15 FT-IR Spectroscopy:

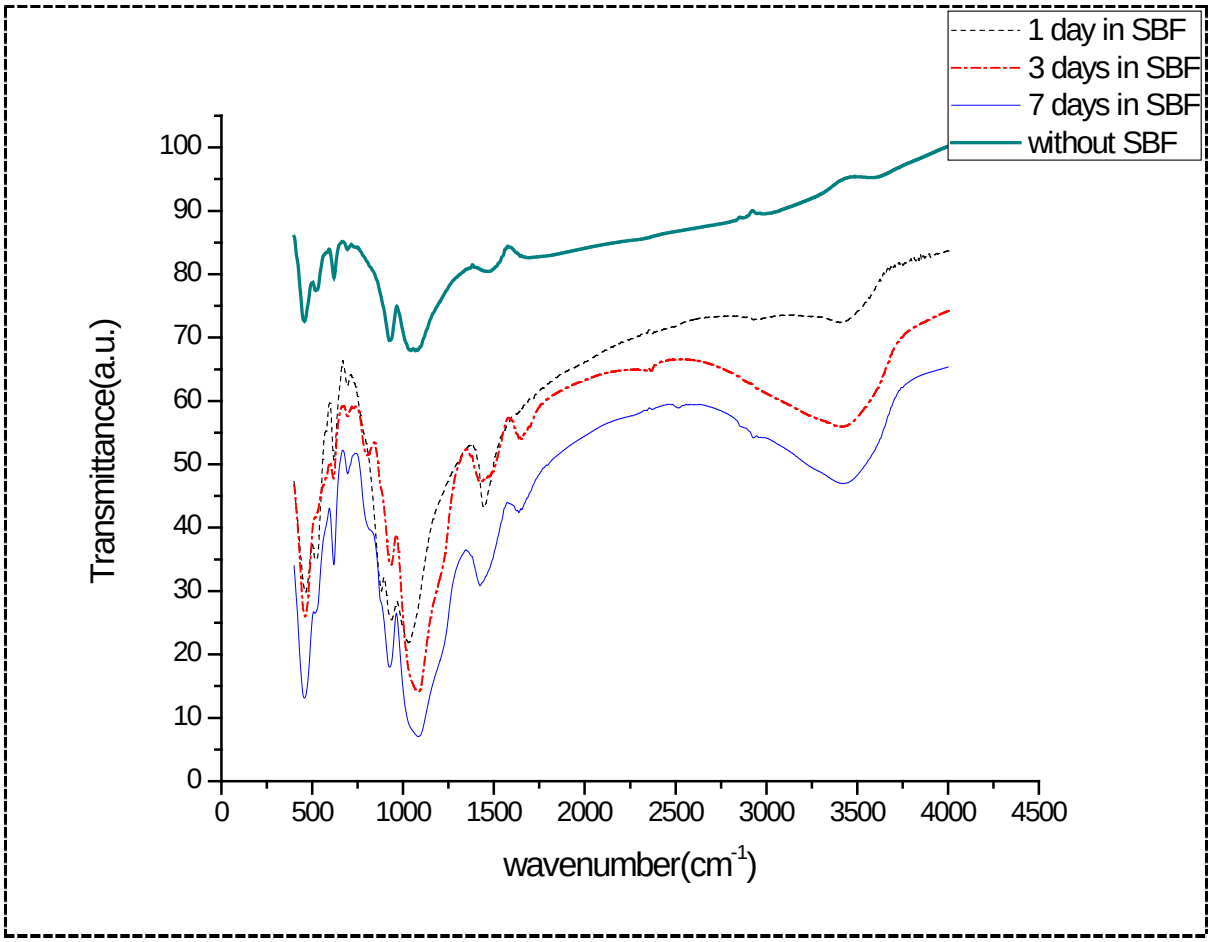

fig 4.17 showing the FTIR curves without immersion in SBF, 1day immersion in SBF, 3 days immersion in SBF, and 7 days immersion in SBF.

From the fig 4.17, it can be observed that:

1) Formation of HCA can be confirmed by the peaks of C=O bond at 144cm^{-1}.
2) P-O bonding vibrations of PO_4 tetrahedra in crystalline apatite can be confirmed by the peaks occouring at 650 cm^{-1}.
3) Phosphate crystallization is marked by the peak at 455 cm^{-1}.
4) Si-O symmetric stretching is shown by the peak at 925 cm^{-1}.
5) Si-O-Si asymmetric stretching is shown by the peak at 1085 cm^{-1}.

CHAPTER 5:
CONCLUSION AND
SCOPE FOR FUTURE WORK

Conclusions

From the results and discussions it can be concluded that the bioactive glass considered for the present work showed very good mechanical properties which were in close proximity of the properties of the cancellous bone. The bioactivity of the specified composition was proved by using SBF solution and testing with SEM, EDX, and FTIR characterizations. It was studied that the mechanical properties of the body can be very precisely tailored by varying the porosity of the whole body or the component layers in case of graded porous bodies.It was observed that the pore size is dependent on the total porosity, and thus can be further increased directly by increasing the total porosity.The pressing load was optimised to be 200MPa as it showed better results. It was also found that on increasing the pressing load to 300MPa, the green body showed defects due to excessive spring-back effect.The sintering temperature was also optimised to be $1050^{o}C$ after firing the bodies at several different temperatures. Two new pressing methods were introduced in the present work, which has not been reported anywhere else.

Scope for Future Work

1. This new pressing method can be tried using better pore formers like PEG microspheres as they have uniform shape and size, which can result in more uniform and narrower pore size distribution.
2. Porosity gradient in lamellar structures can also be prepared and studied for mechanical properties.
3. 3 point bending test and fracture toughness of the present material can be studied.
4. Structures with higher porosity can be tried.

References:

Citations:

[1] L. L. HENCH, R. J . SPLINTER, T. K. GREENLEE and W. C. ALLEN, J. Biomed. Mater. Res. 2 (1971) 117.
[2] D.L. Wheeler, K.E. Stokes, H.M. Park, J.O. Hollinger, J. Biomed. Mater. Res. 35 (1997) 249–254.
[3] D.L. Wheeler, K.E. Stokes, R.G. Hoellrich, D.L. Chamberland, S.W. McLoughlin, J. Biomed. Mater. Res. 41 (1998) 527–533.
[4] L.L. Hench, J. Am. Ceram. Soc. 81 (1998) 1705–1728.
[5] I.D. Xynos, A.J. Edgar, L.D.K. Buttery, L.L. Hench, J.M. Polak, Biochem. Biophys. Res.Commun. 276 (2000) 461–465.
[6] LARRY L. HENCH' and JON K. WEST, Chem. Rev. 90 (1990). 33-72.
[7] Hench LL. Bioceramics. J Am Ceram Soc 1998;81:1705–28.
[8] K.F. Leonga, C.K. Chuaa, N. Sudarmadjia, W.Y. Yeonga.J. Biomed. Mater. Res.1 (2008)140–152.
[9] Oana Bretcanu et al. Journal of the European Ceramic Society 29 (2009) 3299–3306.
[10] L. Lefebvre et al. European Cells and Materials Vol. 11. Suppl. 1, (2006) (page 48).
[11] Qiang Fu et al. Materials Science and Engineering C 31 (2011) 1245–1256
[12] A. CuKneyt Tas. Biomaterials 21 (2000) 1429}1438.
[13] Ohtsuki C, Kokubo T, Yamamuro T. J Non-Cryst Solids 1992;143:84-92.

Other refererencs:

[1] Satadru Kashyap, Kyle Griep, John A. Nychka. Materials Science and Engineering C 31 (2011) 762–769
[2] Qi-Zhi Chen et al. Acta Biomaterialia 6 (2010) 4143–4153
[3] Mohamed N. Rahaman et al. Acta Biomaterialia 7 (2011) 2355–2373
[4] Oscar Peitl,Edgar D. Zanotto, Francisco C. Serbena b, Larry L. Hench. Acta Biomaterialia 8 (2012) 321–332
[5] Frank R. Cichocki Jr and Kevin P. Trumble. J. Am. Ceram. Soc., 81 [6] 1661–64 (1998)
[6] Aldo R. Boccaccini, Melek Erol, Wendelin J. Stark, Dirk Mohn, Zhongkui HongJoão F. Mano. Composites Science and Technology 70 (2010) 1764–1776
[7] J. Suwanprateeb,R. Sanngam, W. Suvannapruk, T. Panyathanmaporn. J Mater Sci: Mater Med (2009) 20:1281–1289
[8] L. Lefebvre et al. Acta Biomaterialia 4 (2008) 1894–1903
[9] HELEN H. LU, SIDDARTH D. SUBRAMONY, MARGARET K. BOUSHELL, and XINZHI ZHANG. Annals of Biomedical Engineering, Vol. 38, No. 6, June 2010 (2010) pp. 2142–2154
[10] Y. H. Hsu ,I. G. Turner ,A. W. Miles. J Mater Sci: Mater Med (2007) 18:2251–2256

[11] J. Ma, C.Z. Chen, D.G. Wang, X.G. Meng, J.Z. Shi.Ceramics International 36 (2010) 1911–1916
[12] Qizhi Z. Chena, Ian D. Thompsonb, Aldo R. Boccaccini, Biomaterials 27 (2006) 2414–2425
[13] Jin Sun et al. Journal of Non-Crystalline Solids 354 (2008) 3799–3805
[14] Bo Lei, Xiaofeng Chen , Yingjun Wang, Naru Zhao, Chang Du, Liming Fang. Journal of Non-Crystalline Solids 355 (2009) 2678–2681
[15] M. Vallet-Regı and A. Ra´mila. Chem. Mater. (2000), 12, 961-965
[16] Gregory J. Brentrupet al. J. Am. Ceram. Soc., 92 [1] (2009) 249–252
[17] Marta Cerruti and Claudio Morterra. Langmuir,20, (2004), 6382-6388
[18] Bo Lei,w Xiaofeng Chen,w Yingjun Wang, Naru Zhao, Chang Du, and Liming Fang. J. Am. Ceram. Soc., 93 [1] 32–35 (2010)